Time integration algorithms for elasto-viscoplastic models with multiple hardening laws for geomaterials: enhancement and comparative study

Jian LI[1] and Zhen-Yu YIN[2,*]

[1] *Assistant Professor, Key Laboratory of Urban Underground Engineering of Ministry of Education, Beijing Jiaotong University, Beijing 100044, China; School of Civil Engineering, Beijing Jiaotong University, Beijing 100044, China.*

[2*] *Associate Professor, Department of Civil and Environmental Engineering, The Hong Kong Polytechnic University, Hung Hom, Kowloon, Hong Kong.*

corresponding author: Zhen-Yu YIN; Tel: +852 3400 8470; Fax: +852 2334 6389; Email: zhenyu.yin@polyu.edu.hk; zhenyu.yin@gmail.com

Abstract: To describe the behaviours of geomaterials such as time-dependency, anisotropy and destructuration, multiple hardening parameters and laws are generally needed for application in advanced elasto-viscoplastic models. Time integration with stress updating is a key step in the application of elasto-viscoplastic models to engineering practice. However, the robustness of time integration algorithms for such complicated models has rarely been studied, creating difficulties in selecting and improving algorithms. This paper focuses on use of three typical implicit time integration algorithms - Katona, Stolle and cutting plane - for integration of an advanced elasto-viscoplastic model. First, all selected algorithms are improved to fit the characteristics of the advanced model with multiple hardening parameters and are combined with adaptive substepping procedures to enhance their performance. Then a step-changed undrained triaxial test is simulated at the integration point level, on the basis of which variations in iteration number and relative error of stresses with step size are investigated and compared. Furthermore, the advanced model using different algorithms is implemented into finite element code, with global convergence and calculation time investigated and compared for two boundary value problems: a biaxial test and an embankment. All comparisons demonstrate that the modified cutting plane algorithm with substepping is the most robust and efficient one, followed by the modified Stolle with substepping and the modified Katona with substepping, for an advanced model with multiple hardening parameters.

Keywords*: viscoplasticity, time-dependency, anisotropy, destructuration, stress integration, finite element method*

Funding

The financial supports provided by the RIF project (Grant No. PolyU R5037-18F) from Research Grants Council (RGC) of Hong Kong and the Fundamental Research Funds for the Central Universities (Grant No. 2019JBM083) are gratefully acknowledged.

Conflicts of interest/Competing interests

On behalf of all authors, the corresponding author states that there is no conflict of interest.

Availability of data and material

Not applicable

Code availability

Not applicable, possible based on request to authors

INTRODUCTION

Geomaterials exhibit not only a time-dependent stress-strain relationship [1-4] but also anisotropy [5-7] and destructuration [8-10]. Various constitutive models have been proposed, such as rate-dependent isotropic models [11-17], rate-dependent anisotropic models [18-20] and models accounting for all three features [21-23]. For the last kind of models, three groups of hardening laws were generally required to determine evolutions of hardening parameters related to the size and inclination of yield/reference surface and the amount of interparticle bonding and debonding or damage, increasing the difficulty of numerical performance for time integration algorithms.

Time integration with stress updating is a key step in the application of elasto-viscoplastic models to engineering practice. A few time integration schemes have been proposed or applied to elasto-viscoplastic models with or without anisotropy and destructuration during past decades. Depending on the derivative of the viscoplastic potential, these time integration algorithms can be classified into two categories: (1) schemes requiring second-order derivative of the viscoplastic potential, such as Katona algorithm [24], Desai algorithm [25] and Stolle algorithm [26] which have been extensively used by Tong and Tuan [27], Yin et al. [28], Karstunen et al. [29] and others, and (2) schemes requiring only first-order derivative of the viscoplastic potential, such as the cutting plane algorithm [30] extended from Ortiz and Simo [31]. In general, the former category is mathematically more rigorous, but the task of evaluating second-order derivative may prove laborious and is best avoided. The Desai algorithm is similar with the Katona algorithm when the integration parameter θ of the latter one is set to 1. The latter category uses Taylor series approximation which is mathematically less rigorous, but the task of only evaluating first-order derivative is simpler. Accordingly, a comparative study should be helpful to choose a suitable algorithm for finite element analysis towards engineering practice.

Most recently, the robustness of these time integration schemes for a simple elasto-viscoplastic model with one single hardening law (i.e. without anisotropy and destructuration) was compared at the integration point and finite element levels by Yin et al. [32], who found that Katona algorithm with θ = 1.0 had better convergence and accuracy than the others, although the unavoidability of obtaining

second-order derivative of viscoplastic potential increases the difficulty of numerical implementation. Use of the cutting plane algorithm without the need for second-order derivative of viscoplastic potential is optional, but its convergence and accuracy are poorer for an elasto-viscoplastic model than for other numerical algorithms. The poor performance could be attributed to the fact that the viscoplastic formulation is not appropriately implemented by the cutting plane algorithm, which has been modified recently by Li and Yin [33] but only for a simple model with one hardening law. However, models that have multiple hardening parameters need more rigorous algorithms, which can be enhanced from and compared with current algorithms. Thus far, current studies have lacked such enhancements and comparisons.

Accordingly, this paper enhances and assesses these time integration schemes using an advanced elasto-viscoplastic model of natural soft clays with multiple hardening laws. Three typical numerical algorithms - Katona, Stolle and cutting plane - are selected and enhanced, with their performance (iteration number, relative error of stresses, global convergence, calculation time, etc.) compared at both the integration stress point and the finite element levels.

TIME INTEGRATION ALGORITHMS

In this study, the ANICREEP model of Yin et al. [23], as a representative elasto-viscoplastic model with multiple hardening laws, is selected as example. Then the enhancement and comparison of three selected typical time integration algorithms are presented through their applications to ANICREEP model.

Brief introduction of adopted elasto-viscoplastic model

The advanced elasto-viscoplastic model (ANICREEP) with multiple hardening parameters and rules for natural soft clays was proposed by Yin et al. [23], which considers the effects of time, anisotropy and destructuration. The framework of the ANICREEP model is briefly described in this section with definitions and determination of all parameters summarised in Table A1.

The strain rate $\dot{\boldsymbol{\varepsilon}}$ is assumed to consist of two parts,

$$\dot{\boldsymbol{\varepsilon}} = \dot{\boldsymbol{\varepsilon}}^{e} + \dot{\boldsymbol{\varepsilon}}^{vp} \tag{1}$$

where the superscripts *e* and *vp* stand, respectively, for the elastic and the viscoplastic strain rate tensors. The viscoplastic strain rate is defined by:

$$\dot{\boldsymbol{\varepsilon}}^{vp} = \mu \langle \Phi \rangle \frac{\partial f_d}{\partial \boldsymbol{\sigma}'} \tag{2}$$

where Φ is the overstress function; f_d is the function of dynamic loading surface corresponding to current stress state; $\boldsymbol{\sigma}'$ is the effective stress tensor and is defined by $\boldsymbol{\sigma}' = \boldsymbol{\sigma} - u_w \boldsymbol{\delta}$ with the total stress tensor $\boldsymbol{\sigma}$, the pore water pressure u_w and the Kronecker's delta $\boldsymbol{\delta}$.

In the present model, the overstress function is given by:

$$\Phi = \left(\frac{p_c^d}{p_c^r} \right)^{\beta} \tag{3}$$

where p_c^d and p_c^r represent the sizes of the dynamic loading surface and the reference surface, respectively (see Fig. 1(a)).

The dynamic loading surface f_d has an inclined ellipsoidal shape (as shown in Fig. 1(a)), and is defined by:

$$f_d = \frac{\frac{3}{2}(\boldsymbol{\sigma}_d - p'\boldsymbol{\alpha}_d) : (\boldsymbol{\sigma}_d - p'\boldsymbol{\alpha}_d)}{(M^2 - \frac{3}{2}\boldsymbol{\alpha}_d : \boldsymbol{\alpha}_d) p'} + p' - p_c^d = 0 \tag{4}$$

where $\boldsymbol{\sigma}_d$ is the deviatoric stress tensor; $\boldsymbol{\alpha}_d$ is the deviatoric fabric tensor. Note that the influence of Lode angle can be introduced by modifying *M* [34-36]. For the simplicity the Lode angle effect is not considered herein since the study focuses on the integration algorithm of the model.

The reference surface has the same shape as the dynamic loading surface but different size defined via p_c^r (as shown in Fig. 1(a)). The intrinsic yield surface is assumed again to have a similar shape, with its size defined via p_{ci}, which is related to the size of the reference yield surface with a bonding parameter χ (see Fig. 1) and expressed by:

$$p_c^r = (1 + \chi) p_{ci} \tag{5}$$

The increment of hardening parameter p_{ci} for the intrinsic yield surface is defined by:

$$\mathrm{d}p_{ci} = p_{ci}\frac{1+e_0}{\lambda_i - \kappa}\mathrm{d}\varepsilon_v^{vp} \tag{6}$$

where ε_v^{vp} denotes the viscoplastic volumetric strain. The increment of bonding parameter is defined by:

$$\mathrm{d}\chi = -\chi\xi\left(\left|\mathrm{d}\varepsilon_v^{vp}\right| + \xi_d \mathrm{d}\varepsilon_d^{vp}\right) \tag{7}$$

where $\left|\mathrm{d}\varepsilon_v^{vp}\right|$ is the absolute value of viscoplastic volumetric strain increment; ε_d^{vp} denotes the viscoplastic deviatoric strain.

The rotational hardening law is defined by [6]:

$$\mathrm{d}\boldsymbol{\alpha}_d = \omega\left[\left(\frac{3\boldsymbol{\sigma}_d}{4p'} - \boldsymbol{\alpha}_d\right)\left\langle \mathrm{d}\varepsilon_v^{vp}\right\rangle + \omega_d\left(\frac{\boldsymbol{\sigma}_d}{3p'} - \boldsymbol{\alpha}_d\right)\mathrm{d}\varepsilon_d^{vp}\right] \tag{8}$$

with $\left\langle \mathrm{d}\varepsilon_v^{vp}\right\rangle = 0$ for $\mathrm{d}\varepsilon_v^{vp} \le 0$ and $\left\langle \mathrm{d}\varepsilon_v^{vp}\right\rangle = \mathrm{d}\varepsilon_v^{vp}$ for $\mathrm{d}\varepsilon_v^{vp} > 0$.

In order to appropriate for numerical methods, the stress and strain variables are hereinafter expressed as vectors, i.e., $\boldsymbol{\sigma}' = [\sigma_x', \sigma_y', \sigma_z', \tau_{xy}, \tau_{yz}, \tau_{zx}]^T$ and $\boldsymbol{\varepsilon} = [\varepsilon_x, \varepsilon_y, \varepsilon_z, \gamma_{xy}, \gamma_{yz}, \gamma_{zx}]^T$. Over one loading step with strain increment $\Delta\boldsymbol{\varepsilon}$ and time increment Δt (i.e., $\Delta\boldsymbol{\varepsilon} = \boldsymbol{\varepsilon}_{n+1} - \boldsymbol{\varepsilon}_n$ and $\Delta t = t_{n+1} - t_n$ with the subscript n representing the number of loading step), the elasto-viscoplastic constitutive relation of ANICREEP model can be obtained by:

$$\Delta\boldsymbol{\sigma}' = \boldsymbol{D}(\Delta\boldsymbol{\varepsilon} - \Delta\boldsymbol{\varepsilon}^{vp}) \tag{9}$$

and

$$\Delta\boldsymbol{\zeta} = \Delta\lambda\boldsymbol{h} \tag{10}$$

with

$$\boldsymbol{\zeta} = \begin{bmatrix} p_{ci} & \chi & \boldsymbol{\alpha}_d \end{bmatrix}^T \tag{11}$$

$$\boldsymbol{h}=\begin{bmatrix} p_{ci}\dfrac{1+e_0}{\lambda_i-\kappa}\dfrac{\partial f_d}{\partial p'} \\ -\chi\xi\left(\left|\dfrac{\partial f_d}{\partial p'}\right|+\xi_d\dfrac{\partial f_d}{\partial q}\right) \\ \omega\left[\left(\dfrac{3\boldsymbol{\sigma}_d}{4p'}-\boldsymbol{\alpha}_d\right)\left\langle\dfrac{\partial f_d}{\partial p'}\right\rangle+\omega_d\left(\dfrac{\boldsymbol{\sigma}_d}{3p'}-\boldsymbol{\alpha}_d\right)\dfrac{\partial f_d}{\partial q}\right] \end{bmatrix} \tag{12}$$

where $\Delta\boldsymbol{\varepsilon}^{vp}$ is the increment of viscoplastic strain by the flow rule $\Delta\boldsymbol{\varepsilon}^{vp}=\Delta\lambda\,\partial f_d/\partial\boldsymbol{\sigma}$; $\Delta\lambda$ is the viscoplastic multiplier with $\Delta\lambda=\dot{\lambda}\Delta t$; $\dot{\lambda}$ is the viscoplastic multiplier rate with $\dot{\lambda}=\mu\Phi$.

The stress-strain relationship of the ANICREEP model is highly nonlinear. Thus, it is necessary to limit the maximum value of step size of strain increments per step to guarantee the performances of algorithms, i.e., convergence and accuracy. Therefore, substepping procedures are also suggested to apply to time integration algorithms.

Enhancement of Katona algorithm: OK-AS and MK-AS

OK-AS: Original Katona algorithm with Adaptive Substepping

Katona [24] proposed an algorithm for elasto-viscoplastic models that uses a step-by-step time integration scheme. Beginning with Eq. (9), according to a one-parameter time integration scheme, the definition of $\Delta\boldsymbol{\varepsilon}_0^{vp}$ for a given calculation step is determined by

$$\Delta\boldsymbol{\varepsilon}^{vp}=\Delta t[(1-\theta)\dot{\boldsymbol{\varepsilon}}_0^{vp}+\theta\dot{\boldsymbol{\varepsilon}}^{vp}] \tag{13}$$

where θ is the integration parameter, which is in the range $0\le\theta\le1$. When $\theta=0$, $\Delta\boldsymbol{\varepsilon}^{vp}$ is determined directly by the known value $\dot{\boldsymbol{\varepsilon}}_0^{vp}$ and Δt, and the integration scheme is explicit which was proven unstable; when $0<\theta<1$, $\Delta\boldsymbol{\varepsilon}^{vp}$ is related to the known value $\dot{\boldsymbol{\varepsilon}}_0^{vp}$ and the unknown value $\dot{\boldsymbol{\varepsilon}}^{vp}$ of the end of the calculation step, and the integration scheme is called semi-implicit which was proven conditional stable; when $\theta=1$, $\Delta\boldsymbol{\varepsilon}^{vp}$ is determined by the unknown value $\dot{\boldsymbol{\varepsilon}}^{vp}$ at the end of the calculation step, and the integration scheme is implicit.

For the last two cases, the solution of $\Delta\boldsymbol{\varepsilon}^{vp}$ could be obtained by an iterative procedure.

Substituting Eq. (13) into Eq. (9) and rearranging gives

$$\boldsymbol{P}(\boldsymbol{\sigma}', \dot{\boldsymbol{\varepsilon}}^{vp}) = \boldsymbol{Q}_0$$
$$\text{with} \begin{cases} \boldsymbol{P} = \boldsymbol{D}^{-1}\boldsymbol{\sigma}' + \Delta t\theta\dot{\boldsymbol{\varepsilon}}^{vp} \\ \boldsymbol{Q}_0 = \Delta\boldsymbol{\varepsilon} - \Delta t(1-\theta)\dot{\boldsymbol{\varepsilon}}_0^{vp} + \boldsymbol{D}_m^{-1}\boldsymbol{\sigma}_0' \end{cases} \tag{14}$$

The solutions of $\boldsymbol{\sigma}'$ could be obtained by an iterative procedure using the Newton-Raphson method. The norm of the correctional stress $\delta\boldsymbol{\sigma}'$ could be chosen as a convergent criterion. The viscoplastic strain rate $\dot{\boldsymbol{\varepsilon}}^{vp}$ and hardening variables $\boldsymbol{\zeta}$ are updated according to the new stress.

To improve the calculation performance, a novel adaptive substepping technique is proposed herein to enhance the original Katona algorithm. The current step size *k'* can be estimated by the norm of trial strain increment $\|\boldsymbol{Q}_0 - \boldsymbol{P}\|$. To control the substepping size, a substepping parameter *k* given by users is introduced. If $k' \le k$ representing that the current step size is small enough as expected, no substepping is then required. Otherwise, a substepping is needed for which α_m representing the size ratio of substepping at current loading step with its range from 0 to 1 is introduced to calculate the sub-step sizes $\alpha_m\Delta\boldsymbol{\varepsilon}$ and $\alpha_m\Delta t$, where the subscript *m* counts the number of the substepping. In order to be adoptive, the value of α_m is estimated by k/k' to make sure that the new sub-step size is within that of expected maximum value.

The flow chart for the original Katona algorithm with adaptive substepping procedure (OK-AS) is presented in Fig. 2, where *TOL* is the tolerance used to judge iterative convergence and the superscript (*i*) represents the *i*th iterative step.

MK-AS: Modified Katona algorithm with Adaptive Substepping

For the original Katona algorithm, only the stress $\boldsymbol{\sigma}'$ is solved by iterative procedure, $\delta\boldsymbol{\sigma}'^{i} = (\boldsymbol{P}')^{-1}(\boldsymbol{Q} - \boldsymbol{P})$, and then the hardening parameters $\boldsymbol{\zeta}$ are updated. According to Eqs. (9) and (10), both $\boldsymbol{\sigma}'$ and $\boldsymbol{\zeta}$ change with viscoplastic strain. For the ANICREEP model, the number of hardening parameters is more than for the simple one, so the iterative procedure ignores $\boldsymbol{\zeta}$ to reduce the convergence rate. The original Katona algorithm could be modified as follows.

Substituting Eq. (13) into Eqs. (9) and (10) gives

$$\bar{\boldsymbol{P}}(\boldsymbol{\sigma}', \boldsymbol{\zeta}, \dot{\boldsymbol{\varepsilon}}^{vp}) = \bar{\boldsymbol{Q}}_0$$

$$\text{with} \begin{cases} \bar{\boldsymbol{P}} = \begin{bmatrix} \boldsymbol{D}^{-1}\boldsymbol{\sigma}' + \Delta t\theta\dot{\boldsymbol{\varepsilon}}^{vp} \\ \boldsymbol{\zeta} - \Delta t\theta\dot{\lambda}\boldsymbol{h} \end{bmatrix} \\ \bar{\boldsymbol{Q}}_0 = \begin{bmatrix} \Delta\boldsymbol{\varepsilon} - \Delta t(1-\theta)\dot{\boldsymbol{\varepsilon}}_0^{vp} + \boldsymbol{D}^{-1}\boldsymbol{\sigma}_0' \\ \boldsymbol{\zeta}_0 + \Delta t(1-\theta)\dot{\lambda}_0\boldsymbol{h}_0 \end{bmatrix} \end{cases} \tag{15}$$

The solutions of $\boldsymbol{\sigma}'$ and $\boldsymbol{\zeta}$ are obtained by an iterative procedure using the Newton-Raphson method, and viscoplastic strain rate $\dot{\boldsymbol{\varepsilon}}^{vp}$ is updated according to the new stress and hardening parameters. The second-order derivative of plastic potential additionally to the hardening parameters used in the modified Katona algorithm is more laborious but more rigorous than in the original Katona algorithm.

Moreover, the novel adaptive substepping technique proposed for the original Katona algorithm is also adopted in the modified one. The flow chart for the modified Katona algorithm with adaptive substepping procedure (MK-AS) is shown in Fig. 3.

Enhancement of Stolle algorithm: MS-AS

Based on the implicit strategy described by Borja and Lee [37] for elastoplastic models, Stolle et al. [26] proposed a time integration algorithm for a viscoplasticity. Unlike the original Katona algorithm, the unknown variable solved by an iterative procedure is the plastic multiplier [37] or the viscoplastic volumetric strain [26] rather than stress [24]. The methods proposed by Borja and Lee [37] and Stolle et al. [26] are not appropriate for the ANICREEP model because of the significant nonlinear variation in the direction of viscoplastic strain under most stress paths. Accordingly, a viscoplastic strain increment consisting of both the inelastic multiplier and the viscoplastic strain rate direction is chosen as the unknown variable solved by an iterative procedure.

When Δt is known, the initial value of $\Delta\boldsymbol{\varepsilon}^{vp0}$ is calculated by the initial stress $\boldsymbol{\sigma}_0'$ and the initial hardening parameters $\boldsymbol{\zeta}_0$ before this loading step. Then the stress $\boldsymbol{\sigma}'$, the hardening parameters $\boldsymbol{\zeta}$ and the viscoplastic strain $\Delta\boldsymbol{\varepsilon}^{vp}$ are

updated according to Eqs. (9) and (10). The target $\Delta\boldsymbol{\varepsilon}^{vp0}$ could be corrected by an iterative procedure using the Newton-Raphson method:

$$\delta\Delta\boldsymbol{\varepsilon}^{vp0} = \frac{\Delta\boldsymbol{\varepsilon}^{vp} - \Delta\boldsymbol{\varepsilon}^{vp0}}{1 - \dfrac{\partial\Delta\boldsymbol{\varepsilon}^{vp}}{\partial\boldsymbol{\sigma}'}\dfrac{\partial\boldsymbol{\sigma}'}{\partial\Delta\boldsymbol{\varepsilon}^{vp0}} - \dfrac{\partial\Delta\boldsymbol{\varepsilon}^{vp}}{\partial\boldsymbol{\zeta}}\dfrac{\partial\boldsymbol{\zeta}}{\partial\Delta\boldsymbol{\varepsilon}^{vp0}}} \tag{16}$$

The norm of the difference between $\Delta\boldsymbol{\varepsilon}^{vp0}$ and $\Delta\boldsymbol{\varepsilon}^{vp}$ could be chosen as a convergent criterion. Moreover, the novel adaptive substepping technique proposed for the original Katona algorithm is also adopted in the modified Stolle algorithm. The current step size *k'* can be estimated by the norm of trial strain increment $\left\|\Delta\boldsymbol{\varepsilon} - \Delta\boldsymbol{\varepsilon}^{vptr}\right\|$ according to the scheme of modified Stolle algorithm. The flow chart for the modified Stolle algorithm with adaptive substepping procedure (MS-AS) is shown in Fig. 4.

Enhancement of cutting plane algorithm: MCP-AS

To seek a simple numerical implementation, the cutting plane algorithm originally proposed by Ortiz and Simo [31] was extended for use in an elasto-viscoplastic model of sand by Higgins et al. [30]. The iterative viscoplastic correction loop requires only the first-order derivative of plastic potential, greatly simplifying implementation. However, the convergence and accuracy of this original cutting plane algorithm for an elasto-viscoplastic model are poorer than those of other numerical algorithms [32]. The poor performance could be attributed to the fact that the viscoplastic formulation is not appropriately implemented in the cutting plane algorithm. To overcome this, an evolution equation for the hardening variable of a dynamic loading surface has been innovatively deduced to develop the modified cutting plane time integration algorithm for a simple elasto-viscoplastic model with one single hardening law (i.e. without anisotropy and destructuration) [33]. Moreover, an adaptive substepping procedure for simultaneously restricting strain and time incremental sizes has been proposed with which to enhance the convergence and accuracy of the modified algorithm. This part extends the modified cutting plane algorithm for ANICREEP model with multiple hardening laws.

Using the definition of the viscoplastic multiplier rate, $\dot{\lambda} = \mu(p_c^d / p_c^r)^\beta$, p_c^d could be expressed by

$$p_c^d = p_c^r \left(\frac{\dot{\lambda}}{\mu} \right)^{1/\beta} \tag{17}$$

The increment of p_c^d could be calculated by

$$\begin{aligned} \mathrm{d}p_c^d &= \frac{\partial p_c^d}{\partial \dot{\lambda}} \mathrm{d}\dot{\lambda} + \frac{\partial p_c^d}{\partial p_c^r} \frac{\partial p_c^r}{\partial \chi} \mathrm{d}\chi + \frac{\partial p_c^d}{\partial p_c^r} \frac{\partial p_c^r}{\partial p_{ci}} \mathrm{d}p_{ci} \\ &= \frac{\partial p_c^d}{\partial \dot{\lambda}} \mathrm{d}\dot{\lambda} + \frac{\partial p_c^d}{\partial p_c^r} \frac{\partial p_c^r}{\partial p_{ci}} \frac{\partial p_{ci}}{\partial \varepsilon_v^{vp}} \dot{\lambda} \mathrm{d}t \frac{\partial f_d}{\partial p'} \\ &+ \frac{\partial p_c^d}{\partial p_c^r} \frac{\partial p_c^r}{\partial \chi} \frac{\partial \chi}{\left| \partial \varepsilon_v^{vp} \right|} \dot{\lambda} \mathrm{d}t \left| \frac{\partial f_d}{\partial p'} \right| + \frac{\partial p_c^d}{\partial p_c^r} \frac{\partial p_c^r}{\partial \chi} \frac{\partial \chi}{\partial \varepsilon_d^{vp}} \dot{\lambda} \mathrm{d}t \frac{\partial f_d}{\partial q} \end{aligned} \tag{18}$$

For a viscoplastic correction loop, the increment of the viscoplastic multiplier rate $\delta\dot{\lambda}^{(i)}$ could be calculated using a Taylor series approximation of the dynamic loading function:

$$\begin{aligned} f_d^{(i+1)} &= f_d^{(i)} + \left(\frac{\partial f_d}{\partial \boldsymbol{\sigma}'} \right)^{(i)} \mathrm{d}\boldsymbol{\sigma}'^{(i)} + \left(\frac{\partial f_d}{\partial p_c^d} \right)^{(i)} \mathrm{d}p_c^{d(i)} + \left(\frac{\partial f_d}{\partial \boldsymbol{\alpha}_d} \right)^{(i)} \mathrm{d}\boldsymbol{\alpha}_d^{(i)} \\ &= f_d^{(i)} - \left(\frac{\partial f_d}{\partial \boldsymbol{\sigma}'} \right)^{(i)} \boldsymbol{D} \left(\frac{\partial f_d}{\partial \boldsymbol{\sigma}'} \right)^{(i)} \Delta t \delta\dot{\lambda}^{(i)} + \left(\frac{\partial f_d}{\partial p_c^d} \frac{\partial p_c^d}{\partial \dot{\lambda}} \right)^{(i)} \delta\dot{\lambda}^{(i)} + \left(\frac{\partial f_d}{\partial \boldsymbol{\zeta}} \frac{\partial \boldsymbol{\zeta}}{\partial \lambda} \right)^{(i)} \Delta t \delta\dot{\lambda}^{(i)} \end{aligned}$$

with (19)

$$\frac{\partial f_d}{\partial \boldsymbol{\zeta}} = \left\{ \frac{\partial f_d}{\partial p_c^d} \frac{\partial p_c^d}{\partial p_c^r} \frac{\partial p_c^r}{\partial p_{ci}}, \frac{\partial f_d}{\partial p_c^d} \frac{\partial p_c^d}{\partial p_c^r} \frac{\partial p_c^r}{\partial \chi}, \frac{\partial f_d}{\partial \boldsymbol{\alpha}_d} \right\},$$

$$\frac{\partial \boldsymbol{\xi}}{\partial \lambda} = \left\{ \frac{\partial p_{ci}}{\partial \varepsilon_v^{vp}} \frac{\partial f_d}{\partial p'}, \frac{\partial \chi}{\partial \varepsilon_v^{vp}} \left| \frac{\partial f_d}{\partial p'} \right| + \frac{\partial \chi}{\partial \varepsilon_d^{vp}} \frac{\partial f_d}{\partial q}, \frac{\partial \boldsymbol{\alpha}_d}{\partial \varepsilon_v^{vp}} \left\langle \frac{\partial f_d}{\partial p'} \right\rangle + \frac{\partial \boldsymbol{\alpha}_d}{\partial \varepsilon_d^{vp}} \frac{\partial f_d}{\partial q} \right\}^T$$

The value of $\delta\dot{\lambda}^{(i)}$ is computed by

$$\delta\dot{\lambda}^{(i)} = \frac{f_d^{(i)}}{\left[\left(\frac{\partial f_d}{\partial \boldsymbol{\sigma}'} \right)^{(i)} \boldsymbol{D} \left(\frac{\partial f_d}{\partial \boldsymbol{\sigma}'} \right)^{(i)} - \left(\frac{\partial p_c^d}{\partial \boldsymbol{\zeta}} \frac{\partial \boldsymbol{\zeta}}{\partial \lambda} \right)^{(i)} \right] \Delta t - \left(\frac{\partial f_d}{\partial p_c^d} \frac{\partial p_c^d}{\partial \dot{\lambda}} \right)^{(i)}} \tag{20}$$

The stress and the hardening variables are updated by

$$\boldsymbol{\sigma}'^{(i+1)} = \boldsymbol{\sigma}'^{(i)} - \Delta t \delta\dot{\lambda}^{(i)} \boldsymbol{D} \left(\frac{\partial f_d}{\partial \boldsymbol{\sigma}'} \right)^{(i)} \tag{21}$$

$$\bar{\boldsymbol{\zeta}}^{(i+1)} = \bar{\boldsymbol{\zeta}}^{(i)} + \left(\frac{\partial \bar{\boldsymbol{\zeta}}}{\partial \dot{\lambda}} \right)^{(i)} \delta\dot{\lambda}^{(i)} + \left(\frac{\partial \bar{\boldsymbol{\zeta}}}{\partial \dot{\lambda}} \right)^{(i)} \Delta t \delta\dot{\lambda}^{(i)} \tag{22}$$

where $\bar{\boldsymbol{\zeta}} = \left[p_c^d \quad p_{ci} \quad \chi \quad \boldsymbol{\alpha}_d \right]^T$.

During the iteration, the value of the dynamic loading function $f_d^{(i+1)}$ is checked. If the stress state is far from the dynamic loading surface, the correction loop will iterate again. If the stress state is near the dynamic loading surface, the algorithm is completed and the updated stress recorded as the output for next loading step.

The novel adaptive substepping technique proposed for the original Katona algorithm is also adopted in the modified cutting plane algorithm. The current step size *k'* can be estimated by the norm of relative trial stress increment $\left\| \boldsymbol{\sigma}'^{tr} - \bar{\boldsymbol{\sigma}}' \right\| / \left\| \bar{\boldsymbol{\sigma}}' \right\|$ according to the scheme of modified cutting plane algorithm, where $\bar{\boldsymbol{\sigma}}'$ presents the image stress point defined by projecting the radial line that connects the origin of coordinate and the initial stress state onto the dynamic loading surface, adjusted by trial stress and hardening parameters. The flow chart for the modified cutting plane algorithm with the adaptive substepping procedure (MCP-AS) is shown in Fig. 5.

NUMERICAL VALIDATION AT THE INTEGRATION POINT LEVEL

To compare the convergence and accuracy of the aforementioned time integration algorithms, a step-changed undrained triaxial test was adopted for use in simulations under the ANICREEP model using different algorithms. The model parameters are based on a series of laboratory tests on Wenzhou sensitive clay [38], summarised in Table 1. For the step-changed undrained triaxial test, both the initial vertical and radial stresses are 1 kPa. The specimen is first compressed to the vertical stress of 75.4 kPa and the radial stress of 41.5 kPa within 3 days. Then the specimen is sheared up to axial strains of 4 %, 8 %, 12 % and 17 % in sequence, with strain rates of 2 %/h, 20 %/h, 0.2 %/h and 2 %/h, respectively.

The substepping parameter *k* restricts the maximum loading step size. Normally, the total iteration number decreases with the increasing of loading step size, however, the relative error of stress increases with the increasing of loading step size [32]. Therefore, an appropriate value of substepping parameter *k* could simultaneously guarantee desired efficiency and accuracy of algorithms. The

converging rate of algorithm only required the first-order derivative of plastic potential is slower than that required the second-order derivative of plastic potential for a given step size. Therefore, a stricter substepping condition is required for the modified cutting plane algorithm. The substepping parameter *k* controls the allowed maximum norm of trial strain increment during trial stage for the original Katona algorithm, the modified Katona algorithm and the modified Stolle algorithm, however, it controls the allowed maximum norm of relative trial stress increment during trial stage for the modified cutting plane algorithm. Therefore, a unified substepping parameter *k* is set to 0.01 for the following simulation at the integration point level, which is strict enough for all algorithms.

During simulations, step sizes of strain increment per step range from 0.01 % to 1 % for undrained triaxial tests (see legends in Fig. 6). To find the relative errors of the calculated results, an ‘‘exact’’ solution is required against which all approximate solutions can be compared. Such a solution is assumed by each time integration method with a small step size, e.g. with a vertical strain increment $\Delta\varepsilon_{ver}$ of 0.0001 % herein. The relative error of stresses is computed by

$$E = \sqrt{\frac{1}{2N}\sum_{i=1}^{N}\left[\left(\frac{p_i' - p_i'^{ex}}{p_i'^{ex}}\right)^2 + \left(\frac{q_i - q_i^{ex}}{q_i^{ex}}\right)^2\right]} \tag{23}$$

where p'^{ex} and q^{ex} are the ‘‘exact’’ solutions and N represents the number of compared stress points.

A comparison of simulations using different time integration methods for the step-changed undrained triaxial test is presented in Fig. 6. First, as shown in Figs. 6 (a) and (b), the performance of convergence for the original Katona algorithm (θ = 0.5) without a substepping procedure is unacceptable. The solutions suddenly deviate exactly when the strain rate decreases from 20 %/h to 0.2 %/h. The deviations of calculated stresses increase with step size, and the calculations cannot converge when step size equals or exceeds 0.1 %. This poor convergence performance is attributable to the generation of substantial viscoplastic strain at the first calculation step, with a strain rate of 0.2 %/h. The original Katona algorithm (θ = 0.5) without a substepping procedure is not appropriate for use in situations featuring large viscoplastic strain, however, in which better performance is achieved by combining a substepping procedure or setting θ = 1 as shown in Figs.

6 (c) to (f). Second, as shown in Figs. 6 (e) to (p), convergence performance for the original and modified Katona algorithms (θ = 1) and for the modified Stollen algorithm is acceptable regardless of whether substepping procedures are applied. Third, convergence performance for the modified cutting plane algorithm without a substepping procedure is the worst: calculations cannot converge even though step size equals 0.01 %, and thus calculation results cannot be illustrated. This poor performance results most probably because the modified cutting plane only uses first-order derivative of viscoplastic potential. As shown in Figs. (q) and (r), convergence performance for the modified cutting plane is much improved by combining it with use of an adaptive substepping procedure.

Variations in iteration number and relative error of stresses with step size for all time integration algorithms are illustrated in Fig. 7. First, as shown in Figs. 7(a) and (b), average iteration numbers increase and total iteration numbers decrease with increasing step size. Second, the iteration numbers for the modified cutting plane algorithm are smaller than for the others in all situations. Third, at the low step size range, the iteration number for the modified Katona algorithm (θ = 1) is similar to that for the original Katona algorithm and the modified Stolle algorithm. However, at the large step size range, the convergence rate for the modified Katona algorithm (θ = 1) is faster than for the original Katona algorithm and the modified Stolle algorithm through application of the second-order derivative of viscoplastic potential to the stress and hardening parameters simultaneously. It is worth mentioning that the iteration number for the modified Katona algorithm without a substepping procedure is less than for the modified cutting plane algorithm when step size equals 0.1 %. In short, for the modified Katona algorithm (θ = 1), the average iteration number's rate of increase with step size is slower than for the others. Fourth, Fig. 7(c) shows that the relative error of stresses for the original Katona algorithm (θ = 0.5) without a substepping procedure is at least two orders of magnitude higher than the original and modified Katona algorithms (θ = 1), the modified Stolle algorithm and the modified cutting plane algorithm at the converged range of step size. The relative error of stresses for the original Katona algorithm (θ = 0.5) is effectively controlled by the substepping procedure. At the large step size range, the relative error of stresses for Katona algorithm (θ = 0.5) combined with a substepping procedure is similar to that for the others.

NUMERICAL VALIDATION AT THE FINITE ELEMENT LEVEL

According to above investigation, all of the above algorithms with adaptive substepping (i.e., OK-AS (θ = 0.5 and 1), MK-AS (θ = 1) , MS-AS, MCP-AS) are selected for further investigation. A user-defined soil model (UDSM) has been developed for the ANICREEP model by employing these time integration algorithms for its use within the commercial finite element code PLAXIS 2D. The model was programmed following the rules of the PLAXIS program for implementing user-defined constitutive models, as stated in the PLAXIS material models manual [39]. Two examples, a biaxial test and an embankment, were simulated and compared by the ANICREEP model using different time integration algorithms. Note that for both cases, reasonable mesh densities are chosen without investigating the problem of mesh-dependency, since the focus is on examining the robustness and efficiency of algorithms.

Numerical simulation of a biaxial test

A biaxial test was simulated by using PLAXIS under fully undrained condition to compare global iteration number and global calculation time by means of the ANICREEP model using different time integration schemes. Numerical simulation of a biaxial test of soil specimens where shear band occurs is an efficient way to examine the performance of integration algorithms. In the biaxial test, the size of the soil specimen is 1.0 m high and 0.5 m wide. For reasons of symmetry, only half the geometry was modelled, as shown in Fig. 8. Two stiff platens on the top and bottom of the specimen have been considered, with full friction between soil and platens. These platens are modelled as linear elastic with a significant higher stiffness than that assigned to the soil material. Model parameters and initial state variables of the soil are the same as that used in previous numerical validations at the integration point level (Table 1). The boundary displacement of the upper platen is restrained in the horizontal direction, and the boundary displacement of the lower platen is restrained in both the vertical and the horizontal directions. The sample consists of 1198 six-noded elements.

The simulation is conducted in four stages. First, the specimen is isotropically compressed to a target stress of 50 kPa within 1 hour. Second, it is loaded to a

vertical displacement increment of 0.04 m with a global strain rate of 1.0 %/h on the top boundary. Third, it is instantaneously unloaded to a vertical displacement increment of 0.03 m. Finally, it is reloaded to a vertical displacement increment of 0.1 m with a higher global strain rate of 10.0 %/h. The substepping parameter k is set to 0.1, 0.01 and 0.001 respectively for this simulation to investigate the effect of k on the performance of the foregoing time integration algorithms.

The simulated results, curves of the vertical force F_v at the top boundary of the specimen versus the vertical displacement U_v, calculated by the ANICREEP model using the time integration algorithms, are illustrated in Fig. 9. The vertical force F_v increases with the vertical displacement U_v up to a certain vertical displacement, reaching a peak value, and then is gradually attenuated with the formation of the shear band. For the reloading part, the vertical force goes higher than that before unloading due to a higher displacement rate, and then gradually decreases with an obvious strain-softening behaviour. The simulated curves of F_v –U_v are almost the same for different algorithms, except for those with problem of convergence (i.e. OK-AS (θ = 0.5) with all the set value of k, OK-AS (θ = 1.0) with k = 0.1 and 0.01, MS-AS with k = 0.1).

The results calculated by the different algorithms are similar, so only that one calculated using the modified Katona algorithm (θ = 1) with k = 0.01 is illustrated in Fig. 10. Fig. 10(a) shows the true scale deformed mesh after the shearing stage, up to a global vertical strain of 10 %. The soil specimen is cut into three parts, the bottom, middle and upper, by a couple crossed shear bands. The middle triangular part moves right, and the upper part shifts down. Fig. 10(b) shows that two crossed shear bands expressed by shear strain (or deviatoric strain) are clearly located in the lower half of the specimen. Their widths are almost equal to that of the two elements. The shear strain exceeds 100 % in most regions of the shear band, and the maximum value of the shear strain in the cross point of the two shear bands is nearly 300 %. Fig. 10(c) shows the shading of bonding ratio χ after the shearing stage. According to Eq. (7), the bonding ratio χ decreases with increasing viscoplastic strain. It is then reasonable for the values of bonding ratio χ of elements located at shear bands to be nearly zero.

The total number of iterations and central processing unit (CPU) time calculated by the ANICREEP model using different time integration schemes are summarised in Table 2 for comparison. First, the performance of the original

Katona algorithm (θ = 0.5) is unacceptable. All simulations using the original Katona algorithm (θ = 0.5) with a substepping procedure failed, with non-convergence seen during the loading and reloading stage. The final vertical displacement increment corresponding to simulated non-convergence increases with decreases in substepping parameter *k*. The performance of the original Katona algorithm is slightly improved by setting θ = 1. The simulation using the original Katona algorithm (θ = 1) with *k* = 0.001 is completed. Second, the performance of the modified Stolle algorithm exceeds that of the original Katona algorithm. Its simulations are completed with *k* = 0.01 and 0.001. Third, all simulations using the modified Katona algorithm (θ = 1) and the modified cutting plane algorithm are completed. Their simulations with the smallest value of *k*, i.e., *k* = 0.001 are not carried out. It is worth noting that the simulations using the modified Katona algorithm (θ = 1) without a substepping procedure are also completed, although this is not illustrated in Table 3. The number of iterations for the modified Katona algorithm (θ = 1) is smaller than for the modified cutting plane algorithm, and the difference in iteration number between the modified Katona algorithm (θ = 1) and the modified cutting plane algorithm drops with decreases in substepping parameter *k*. However, the CPU time for the modified Katona algorithm (θ = 1) is one order larger than for the modified cutting plane algorithm. The substantial CPU time required for the modified Katona algorithm (θ = 1) could be attributable to the requirement of matrix inversion, which is 15 rows and 15 columns, for six deviatoric stress tensor σ_d components, one mean effective stress *p'*, one hardening parameter p_{ci}, one hardening parameter χ and six deviatoric fabric tensor α_d components.

Additional simulations of biaxial testing with target vertical displacement U_y at the top boundary of 0.5 m using different algorithms were carried out to investigate the robustness of its capacity for large deformation analysis. Vertical displacements until calculation of non-convergence U_{ync} using different time integration methods are summarised in Table 3 for comparison. The value of U_{ync} increases with substepping parameter *k* for all algorithms. In descending value of U_{ync}, algorithms range from the cutting plane algorithm, the modified Katona algorithm with θ = 1, and the modified Stolle algorithm to the original Katona algorithm with θ = 1 and then with θ = 0.5. It is worth noting that only those

calculations using the modified Katona algorithm with $\theta = 1$ and the modified cutting plane have been completed with given substepping parameter k.

Numerical simulation of an embankment on soft clay

To further examine the performance of different algorithms applied to the ANICREEP model coupled with Biot's consolidation analysis, a simplified embankment example on soft clay, presented by Karstunen et al. [40], was adopted and simulated using PLAXIS to compare global iteration number and global calculation time under the ANICREEP model using different time integration methods. The soft soil is assumed to have the properties of Poko clay from Finland. Model parameters and initial state variables of soil are listed in Table 4. The embankment, assumed to be made of granular fill, is modelled using a simple Mohr Coulomb model, assuming the material parameters E = 40 000 kN/m^2, ν = 0.3, $\varphi = 38°$, $\psi = 0°$, c = 1 kN/m^2 and $\gamma = 20$ kN/m^3, where E is the Young's modulus, ν the Poisson's ratio, φ the internal friction angle, ψ the dilatancy angle, c the cohesion and γ the unit weight of the embankment material. The geometry of the embankment is shown in Fig. 11. The groundwater table is located 2 m below the ground surface. Drained conditions and zero initial pore pressures are assumed to be above the water table. The domain to be analysed (under plane strain conditions) extends 60 m in the horizontal direction from the symmetry axis and 36 m in the vertical. The lateral boundaries are restrained horizontally, and the bottom boundary is restrained in both directions. Drainage boundaries are assumed to be at the level of the water table and at the bottom of the mesh. For reasons of symmetry, only half the embankment is represented in the finite element model. A mesh with 739 six-noded triangular elements has been used in all analyses, with extra degrees of freedom for excess pore pressures at corner nodes. The generated element number is slightly more than in the embankment example given by Karstunen et al. [40].

According to Karstunen et al. [40], embankment loading is first applied under undrained conditions, assuming the embankment and the soil above the water table to be drained materials. Next a consolidation phase is simulated via fully coupled static consolidation analyses. The problem was modelled using small strain analyses, for large strain analyses produced only marginally different results and the focus is on examining the robustness and efficiency of algorithms. Although the

simulation of the biaxial test by the modified Katona algorithm (θ = 0.5 and 1) with k = 0.01 are not converged, the viscoplastic volumetric or shear strains generated in this simulation of the embankment will be not as significant as that generated for the prior example. Therefore, the substepping parameter k is set to 0.01 for this simulation.

The simulated results produced by the foregoing time integration algorithms are presented in Fig. 12 for 2 days of loading time and 100 years of consolidation time, conditions that produce almost identical results. The vertical displacement U_v at point A at the centre of the embankment base increases with time, and its value is about 1.2 m at 100 years. The excess pore pressure p_w at point B, 6 m under the centre of the embankment base, is generated during the construction stage and dissipates with time during the consolidation stage, and its value is nearly 2 kPa at 100 years. The horizontal displacement U_h at point C, 6 m under the slope toe of the embankment, increases with time, and its value is about 0.07 m at 100 years.

The simulated excess pore water pressure field after the construction stage and the simulated displacement field after 100 years of consolidation are similar when calculated using different algorithms. Thus only the results calculated using the modified Katona algorithm (θ = 1) with k = 0.01 are illustrated in Fig. 13. Fig. 13 (a) shows that the excess pore water pressure of nodes at the top of layers 2 and 3 near the centreline of the embankment is large after the construction stage but decreases with distance from the bottom of the embankment. The maximum excess pore water pressure is nearly 38 kPa. Fig. 13(b) shows that the maximum displacement of nodes at the centre of the embankment bottom is nearly 1.4 m, with displacement decreasing with distance from the bottom of the embankment.

The total number of iterations and central processing unit (CPU) time calculated by the model using different time integration methods are summarised in Table 5 for comparison. The number of iterations calculated using different algorithms is similar. However, the CPU time calculated using different algorithms is not the same, so that the CPU time calculated by the modified cutting plane algorithm is the shortest, with that calculated by the modified Katona algorithm (θ = 1) the longest. For instance, the calculated CPU time of modified Katona algorithm (θ = 1) is nearly 16 times that using the modified cutting plane algorithm.

DISCUSSION

Based on the preceding numerical analysis, the performance of all time integration algorithms is summarised in Table 6. At the integration point level, convergence performance for the original Katona algorithm (θ = 0.5) without a substepping procedure is unacceptable but is improved by setting θ = 1 and combining a substepping procedure. The performance of convergence and accuracy of the original Katona algorithm (θ = 0.5) with a substepping procedure, the original and modified Katona algorithms (θ = 1) with and without a substepping procedure, the modified Stolle algorithms with and without a substepping procedure and the modified cutting plane algorithm with a substepping procedure are good.

At the finite element level, convergence performance for all algorithms without substepping procedures is unacceptable, save for the modified Katona algorithm (θ = 1). Convergence performance for the modified Stolle algorithm and the cutting plane algorithm are improved by substepping procedures. However, the improvement of convergence for the original Katona algorithm (θ = 0.5 and 1) is still unsatisfactory. What's more, the performance of CPU time for the modified cutting plane algorithm is the best for both examples at the finite element level.

CONCLUSIONS

Implicit numerical algorithms with enhancements proposed in this study – the original Katona algorithm, the modified Katona algorithm, the modified Stolle algorithm and the modified cutting plane algorithm – were applied to the advanced elasto-viscoplastic model ANICREEP with three hardening parameters. These implicit algorithms can be classified into two categories: (1) in the first category, the original Katona algorithm, the modified Katona algorithm and the modified Stolle algorithm, the second-order derivative of the viscoplastic potential is required, which is laborious and best avoided but rigorous; (2) in the second category, the modified cutting plane algorithm, only the first-order derivative of viscoplastic potential is required for an iterative viscoplastic correction loop, greatly simplifying model implementation but with less rigorous.

At the integration point level, the step-changed undrained triaxial test was selected for use in simulation to compare the convergence and accuracy of the aforementioned time integration algorithms. First, use of the original Katona

algorithm (θ = 0.5) without a substepping procedure is not appropriate for use in situations featuring large viscoplastic strains, in which performance is improved by combining a substepping procedure or setting θ = 1. Second, the performance of the original and modified Katona algorithms (θ = 1) with and without a substepping procedure, the modified Stolle algorithm with and without a substepping procedure, and the modified cutting plane algorithm with a substepping procedure are acceptable. Their average iteration numbers increase, the total iteration numbers decrease, and the relative errors of stresses increase with step size.

At the finite element level, a biaxial test and an embankment were simulated using finite element method, with which models using different algorithms were implemented. Global iteration number and global calculation time were compared for all algorithms. First, convergence performance for all algorithms without substepping is unacceptable except for the modified Katona algorithm (θ = 1) without substepping. Except for the original Katona algorithm (θ = 1 and 0.5), convergence performance is improved by use of substepping procedures for the biaxial test with occurring shear band. Second, performance of CPU time for the modified cutting plane algorithm is the best for both examples at the finite element level.

ACKNOWLEDGMENTS

The financial supports provided by the RIF project (Grant No. PolyU R5037-18F) from Research Grants Council (RGC) of Hong Kong and the Fundamental Research Funds for the Central Universities (Grant No. 2019JBM083) are gratefully acknowledged.

APPENDIX: MODEL PARAMETERS OF ANICREEP

State parameters and constants of ANICREEP model are summarised in Table A1 with their definitions and determination methods. Alternatively, these parameters can also be easily identified by optimization methods as demonstrated by Yin et al. [38] and Jin and Yin [41].

REFERENCES

1. Leroueil S, Kabbaj M, Tavenas F, Bouchard R (1985) Stress-strain-strain rate relation for the compressibility of sensitive natural clays. Géotechnique 35(2):159-180. https://doi.org/10.1680/geot.1985.35.2.159.
2. Yin JH, Cheng CM (2006) Comparison of strain-rate dependent stress-strain behavior from K_0-consolidated compression and extension tests on natural Hong Kong Marine deposits. Mar Georesour Geotec 24(2):119-147. https://doi.org/10.1080/10641190600704780
3. Yin Z-Y, Zhu QY, Yin JH, Ni Q (2014) Stress relaxation coefficient and formulation for soft soils. Géotech Lett 4(1):45-51. https://doi.org/10.1680/geolett.13.00070
4. Zhu QY, Yin Z-Y, Hicher PY, Shen SL (2016) Nonlinearity of one-dimensional creep characteristics of soft clays. Acta Geotech 11(4):887-900. https://doi.org/10.1007/s11440-015-0411-y
5. Díaz Rodríguez JA, Leroueil S, Alemán JD (1992) Yielding of Mexico City clay and other natural clays. J Geotech Engrg 118(7):981-995. https://doi.org/10.1061/(ASCE)0733-9410(1992)118:7(981)
6. Wheeler SJ, Näätänen A, Karstunen M, Lojander M (2003) An anisotropic elastoplastic model for soft clays. Can Geotech J 40(2):403-418. https://doi.org/10.1139/t02-119
7. Yin Z-Y, Chang CS, Hicher P-Y, Karstunen M (2009) Micromechanical analysis of kinematic hardening in natural clay. Int J Plasticity 25(8):1413-1435. https://doi.org/10.1016/j.ijplas.2008.11.009
8. Burland JB (1990) On the compressibility and shear strength of natural clays. Géotechnique 40(3):329-378. https://doi.org/10.1680/geot.1990.40.3.329
9. Leroueil S, Vaughan PR (1990) The general and congruent effects of structure in natural soils and weak rocks. Géotechnique 40(3):467-488. https://doi.org/10.1680/geot.1990.40.3.467
10. Yin Z-Y, Hattab M, Hicher P-Y (2011a) Multiscale modeling of a sensitive marine clay. Int J Numer Anal Meth Geomech 35(15):1682-1702. https://doi.org/10.1002/nag.977
11. Kutter BL, Sathialingam N (1992) Elastic-viscoplastic modelling of the rate-dependent behaviour of clays. Géotechnique 42(3):427-441. https://doi.org/10.1680/geot.1992.42.3.427
12. Vermeer PA, Neher HP (1999) A soft soil model that accounts for creep. In: Proc. Plaxis Symposium 'Beyond 2000 in Computational Geotechnic'. pp 249-262.
13. Yin JH, Zhu JG, Graham J (2002) A new elastic viscoplastic model for time-dependent behaviour of normally and overconsolidated clays: theory and verification. Can Geotech J 39(1):157-173. https://doi.org/10.1139/t01-074
14. Rocchi G, Fontana M, Da Prat M (2003) Modelling of natural soft clay destruction processes using viscoplasticity theory. Géotechnique 53(8):729-745. https://doi.org/10.1680/geot.2003.53.8.729
15. Kelln C, Sharma J, Hughes D, Graham J (2009) Finite element analysis of an embankment on a soft estuarine deposit using an elastic-viscoplastic soil model. Can Geotech J 46(3):357-368. https://doi.org/10.1139/T08-129

16. Yin Z-Y, Hicher P-Y (2008) Identifying parameters controlling soil delayed behaviour from laboratory and in situ pressuremeter testing. Int J Numer Anal Meth Geomech 32(12):1515-1535. https://doi.org/10.1002/nag.684
17. Hinchberger SD, Qu G (2009) Viscoplastic constitutive approach for rate-sensitive structured clays. Can Geotech J 46(6):609-626. https://doi.org/10.1139/T08-133
18. Zhou C, Yin JH, Zhu JG, Cheng CM (2005) Elastic anisotropic viscoplastic modeling of the strain-rate-dependent stress-strain behaviour of K_0-consolidated natural marine clays in triaxial shear tests. Int J Geomech ASCE 5(3):218-232. https://doi.org/10.1061/(ASCE)1532-3641(2005)5:3(218)
19. Leoni M, Karstunen M, Vermeer PA (2008) Anisotropic creep model for soft soils. Géotechnique 58(3):215-226. https://doi.org/10.1680/geot.2008.58.3.215
20. Yin Z-Y, Chang CS, Karstunen M, Hicher P-Y (2010) An anisotropic elastic-viscoplastic model for soft clays. Int J Solid Struct 47(5):665-677. https://doi.org/10.1016/j.ijsolstr.2009.11.004
21. Kimoto S, Oka F (2005) An elasto-viscoplastic model for clay considering destructuralization and consolidation analysis of unstable behaviour. Soils Found 45(2):29-42. https://doi.org/10.3208/sandf.45.2_29
22. Karstunen M, Yin Z-Y (2010) Modelling time-dependent behaviour of Murro test embankment. Géotechnique 60(10):735-749. https://doi.org/10.1680/geot.8.P.027
23. Yin Z-Y, Karstunen M, Chang CS, Koskinen M, Lojander M (2011b). Modeling time-dependent behavior of soft sensitive clay. J Geotech Geoenviron Eng ASCE 137(11):1103-1113. https://doi.org/10.1061/(ASCE)GT.1943-5606.0000527
24. Katona MG (1984) Evaluation of viscoplastic cap model. J Geotech Engrg ASCE 110(8):1106-1125.
25. Desai CS, Zhang D (1987) Viscoplastic model for geologic materials with generalized flow rule. Int J Numer Anal Meth Geomech 11(6):603-620.
26. Stolle DFE, Vermeer PA, Bonnier PG (1999) Time integration of a constitutive law for soft clays. Commun Numer Meth Engng 15(8):603-609.
27. Tong X, Tuan CY (2007) Viscoplastic cap model for soils under high strain rate loading. J Geotech Geoenviron Eng 133(2):206-214. https://doi.org/10.1061/(ASCE)1090-0241(2007)133:2(206)
28. Yin Z-Y, Yin J-H, Huang H-W (2015) Rate-dependent and long-term yield stress and strength of soft Wenzhou marine clay: experiments and modeling. Mar Georesour Geotec, 33(1):79-91. https://doi.org/10.1080/1064119X.2013.797060
29. Karstunen M, Rezania M, Sivasithamparam N, Yin Z-Y (2015) Comparison of anisotropic rate-dependent models for modeling consolidation of soft clays. Int J Geomech ASCE 15(5):A4014003. https://doi.org/10.1061/(ASCE)GM.1943-5622.0000267
30. Higgins W, Chakraborty T, Basu D (2013) A high strain-rate constitutive model for sand and its application in finite-element analysis of tunnels subjected to blast. Int J Numer Anal Meth Geomech, 37(15):2590-2610. https://doi.org/10.1002/nag.2153

31. Ortiz M, Simo JC (1986) An analysis of a new class of integration algorithms for elastoplastic constitutive relations. Int J Numer Meth Engng 23(3):353-366. https://doi.org/10.1002/nme.1620230303
32. Yin Z-Y, Li J, Jin Y-F, Liu F-Y. (2019) Estimation of robustness of time integration algorithms for elasto-viscoplastic modeling of soils. Int J Geomech 19(2):04018197. https://doi.org/10.1061/(ASCE)GM.1943-5622.0001351
33. Li J, Yin Z-Y (2020) A modified cutting-plane time integration scheme with adaptive substepping for elasto-viscoplastic models. Int J Numer Methods Eng, revised.
34. Sheng D, Sloan SW, Yu HS (2000) Aspects of finite element implementation of critical state models. Comput Mech 26:185-196. https://doi.org/10.1007/s004660000166
35. Yao Y, Sun D, Luo T (2004) A critical state model for sands dependent on stress and density. Int J Numer Anal Meth Geomech 28(4):323-337. https://doi.org/10.1002/nag.340
36. Yao Y, Sun D, Matsuoka H (2008) A unified constitutive model for both clay and sand with hardening parameter independent on stress path. Comput Geotech 35(2): 210-222. https://doi.org/10.1016/j.compgeo.2007.04.003
37. Borja RI, Lee SR (1990) Cam-clay plasticity, part 1: implicit integration of elasto-plastic constitutive relations. Comput Methods Appl Mech Engrg, 78(1):49-72. https://doi.org/10.1016/0045-7825(90)90152-C
38. Yin Z-Y, Jin Y-F, Shen S-L, Huang H-W (2017) An efficient optimization method for identifying parameters of soft structured clay by an enhanced genetic algorithm and elastic-viscoplastic model. Acta Geotech, 12(4):849-867. https://doi.org/10.1007/s11440-016-0486-0
39. Plaxis (2012) PLAXIS material models manual. Delft, Netherlands.
40. Karstunen M, Wiltafsky C, Krenn H, Scharinger F, Schweiger HF (2006) Modelling the behaviour of an embankment on soft clay with different constitutive models. Int J Numer Anal Meth Geomech 30(10):953-982.
41. Jin YF, Yin Z-Y (2020) Enhancement of backtracking search algorithm for identifying soil parameters. Int J Numer Anal Meth Geomech. https://doi.org/10.1002/nag.3059.

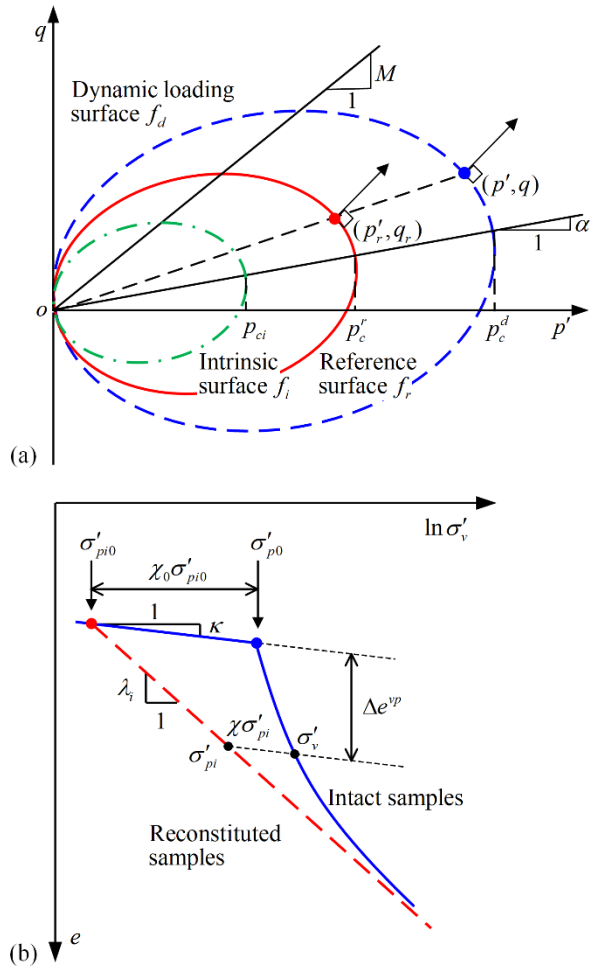

Figure 1 Principle of ANICREEP model (a) definitions for the model in the p'-q plane; (b) schematic plot for one-dimensional compression behaviour

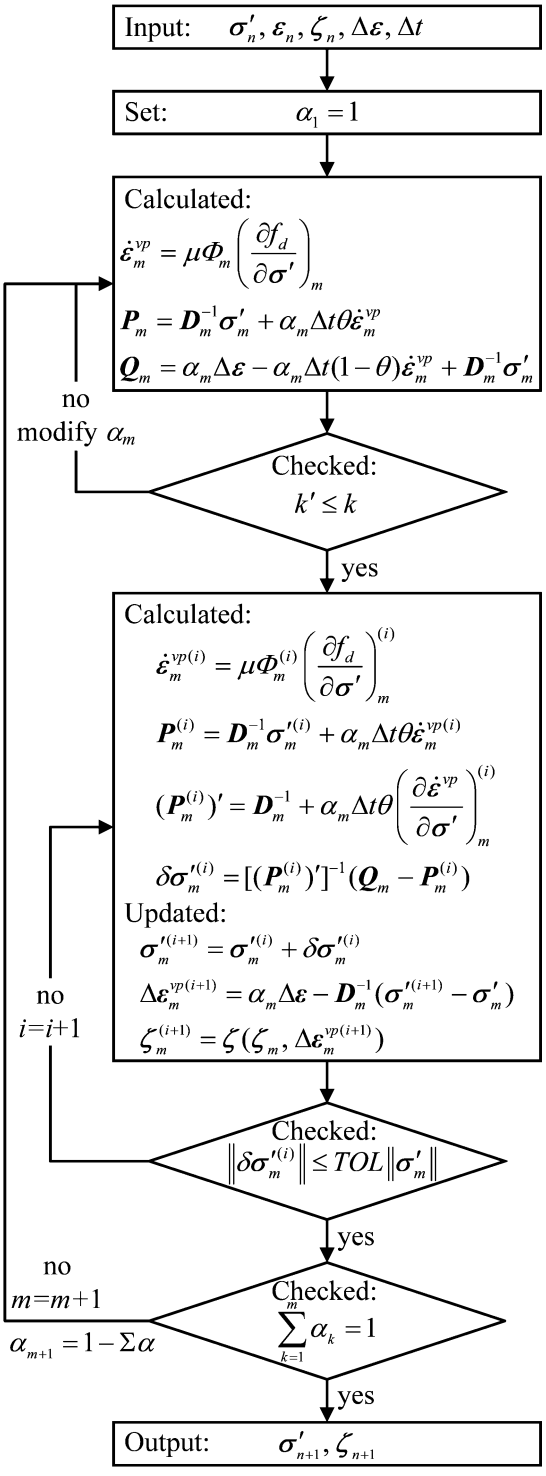

Figure 2 Flow chart of original Katona algorithm with adaptive substepping procedure

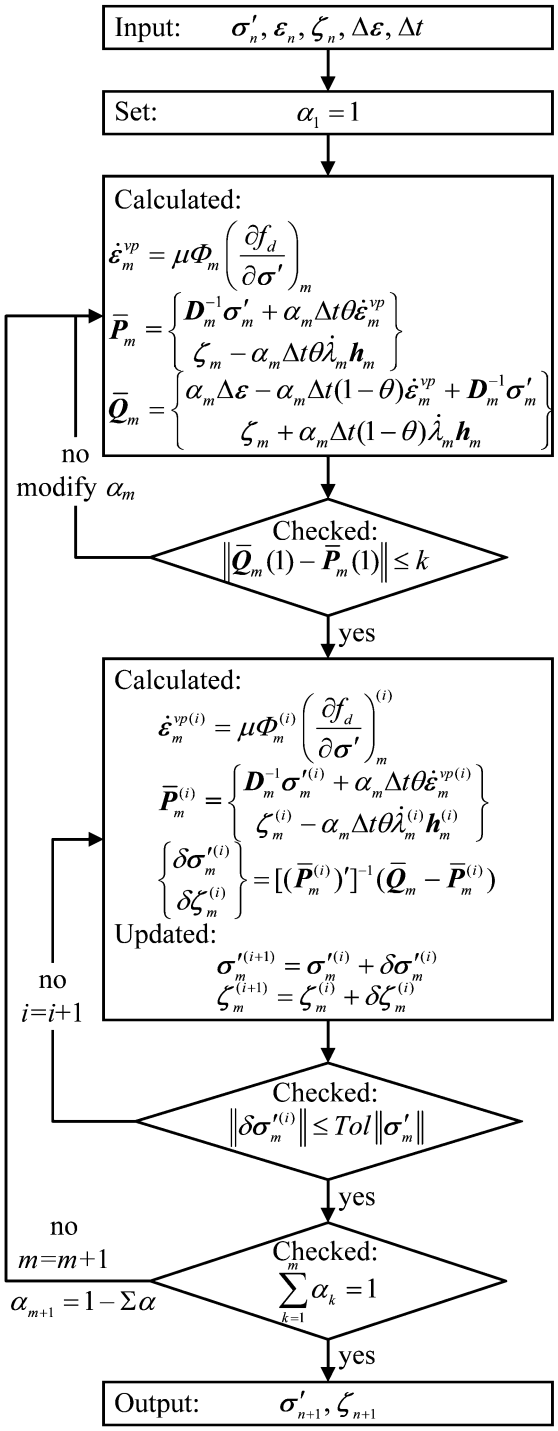

Figure 3 Flow chart of modified Katona algorithm with adaptive substepping procedure

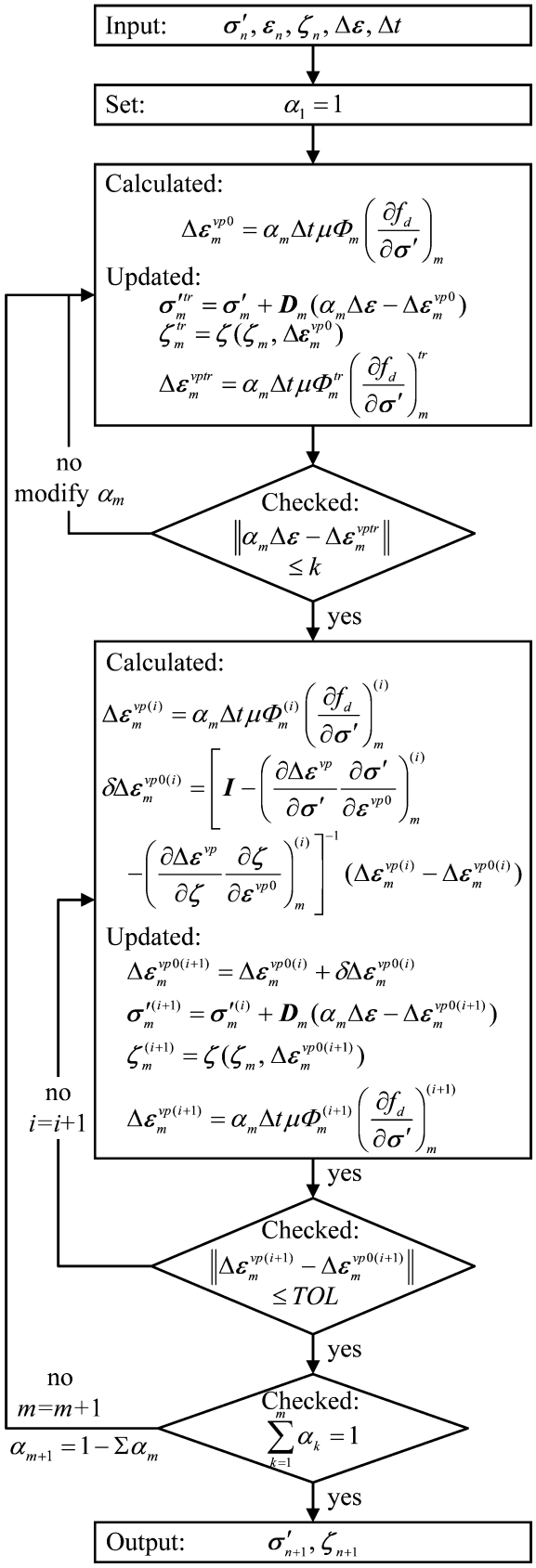

Figure 4 Flow chart of modified Stolle algorithm with adaptive substepping procedure

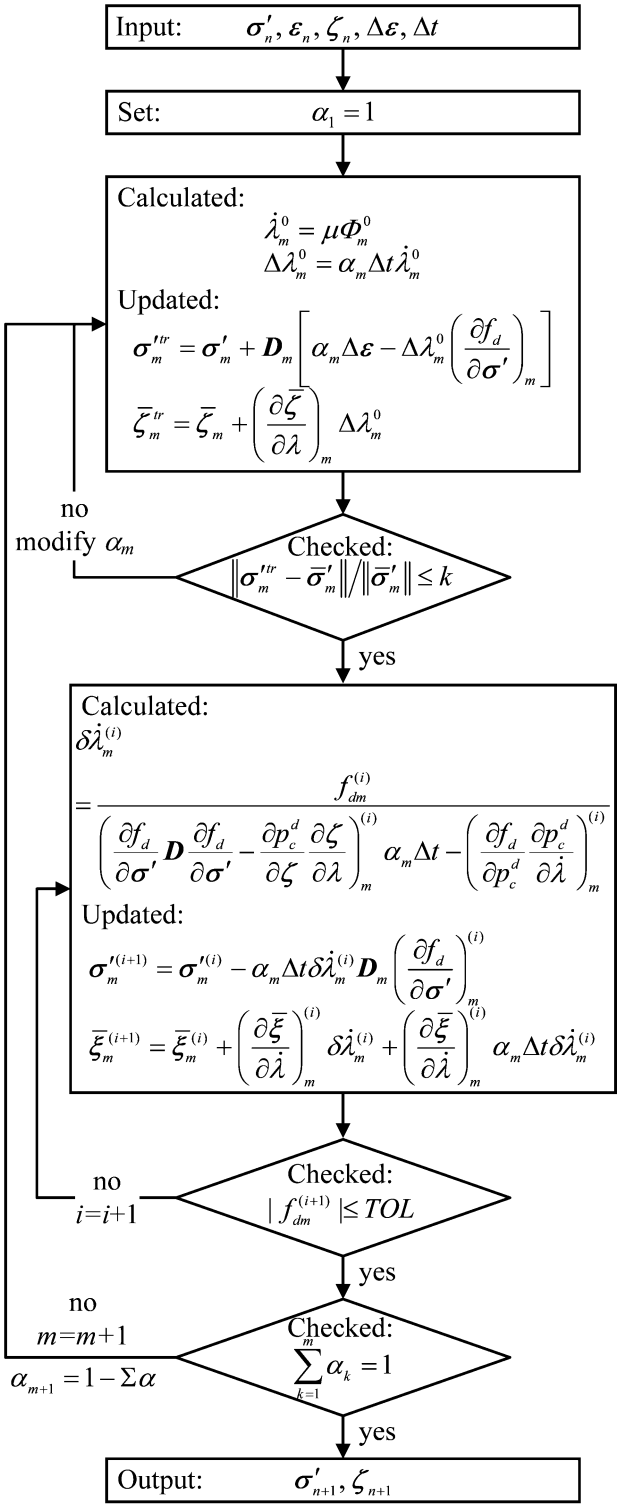

Figure 5 Flow chart of modified cutting plane algorithm with adaptive substepping procedure

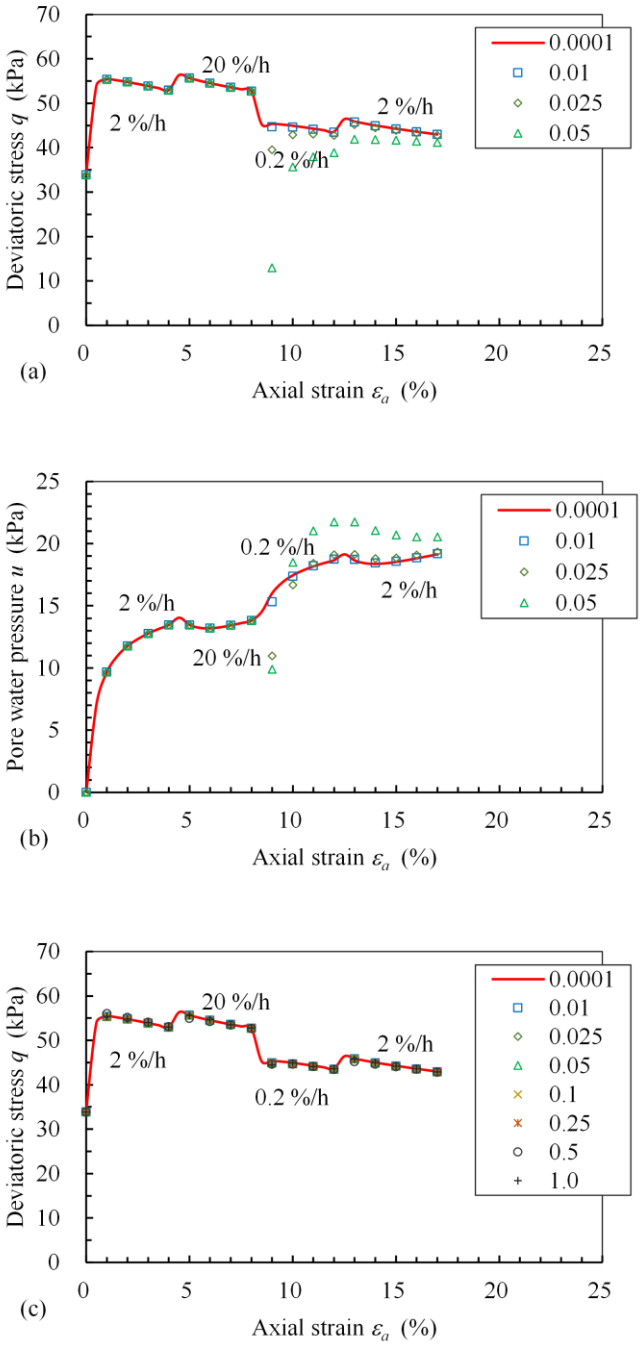

Figure 6 Comparison of simulated results for undrained triaxial step-changed CRS tests by algorithms: original Katona ($\theta = 0.5$) (a-b) without substepping and (c-d) with k = 0.01; original Katona ($\theta = 1$) (e-f) without substepping and (g-h) with k = 0.01; modified Katona ($\theta = 1$) (i-j) without substepping and (k-l) with k = 0.01; modified Stolle (m-n) without substepping and (o-p) with k = 0.01; (q-r) modified cutting plane with k = 0.01.

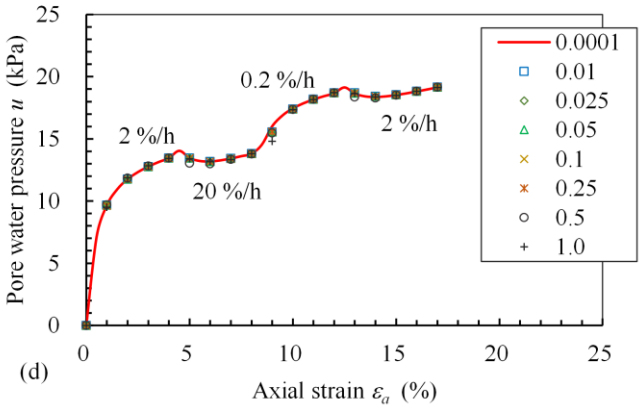

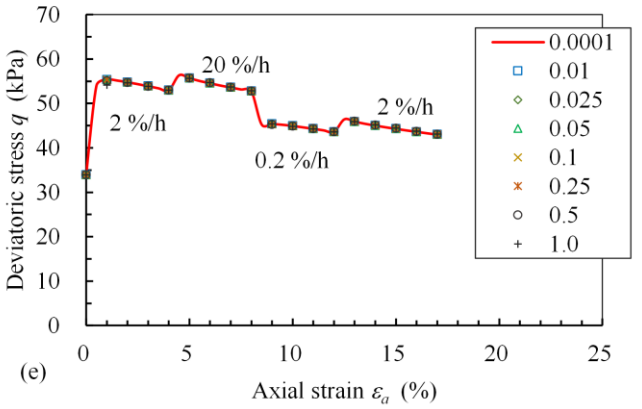

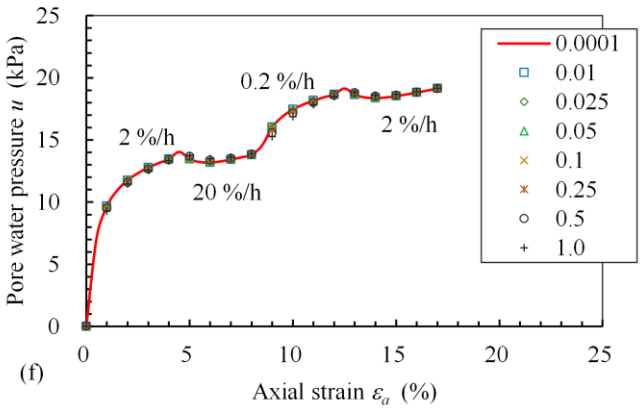

Figure 6 (*Continued*)

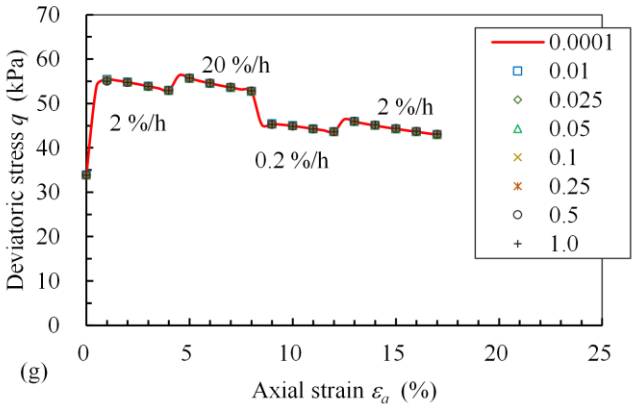

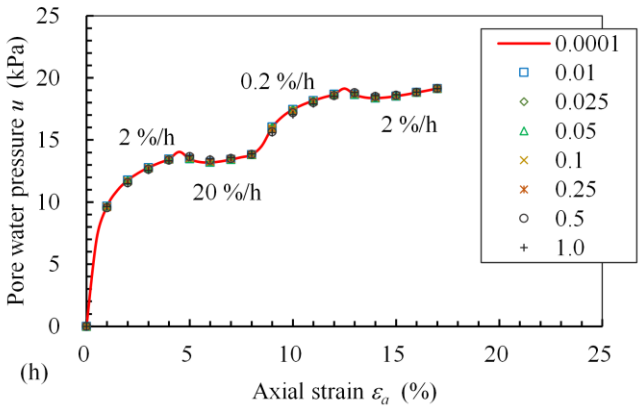

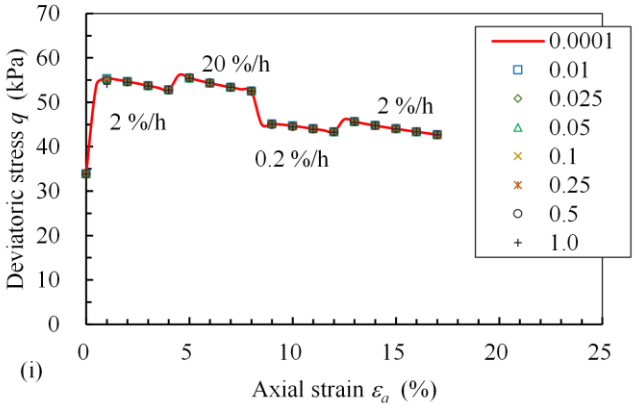

Figure 6 (*Continued*)

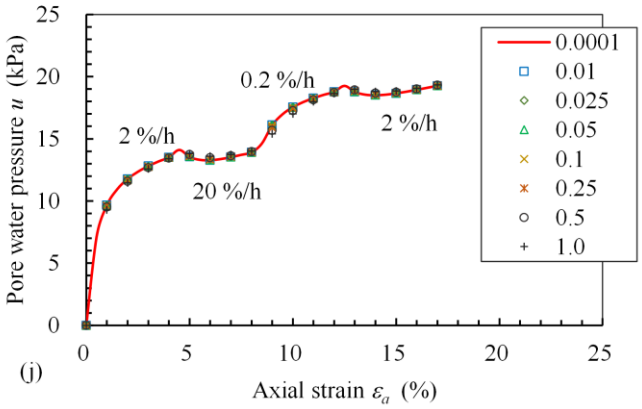

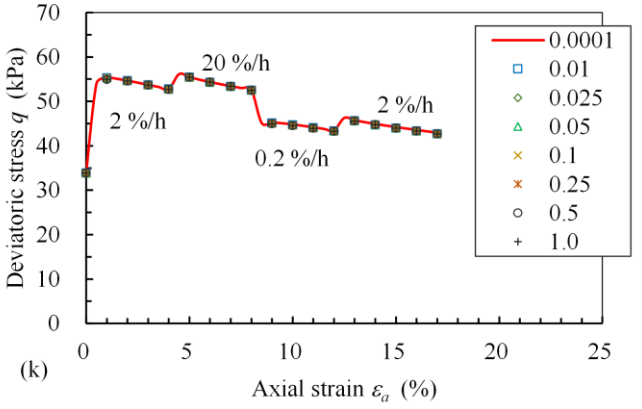

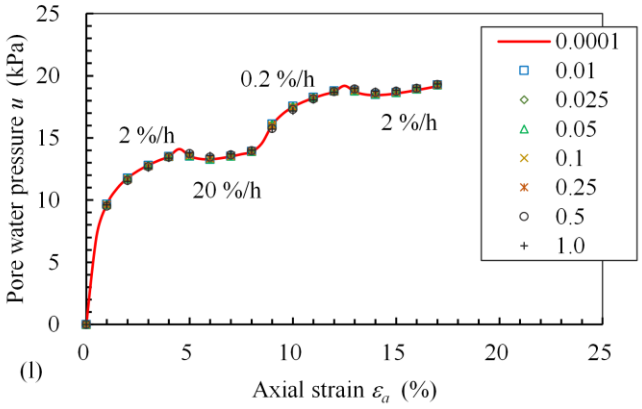

Figure 6 (*Continued*)

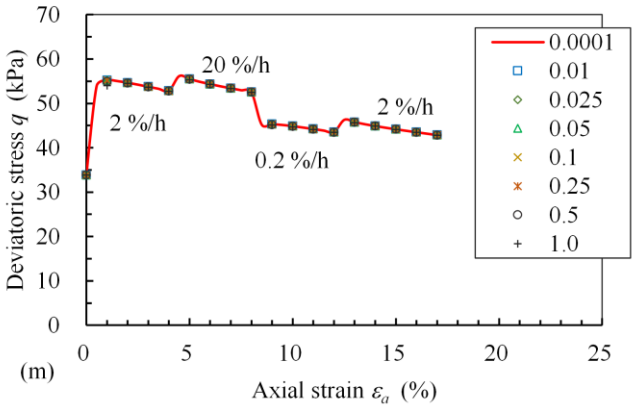

(m)

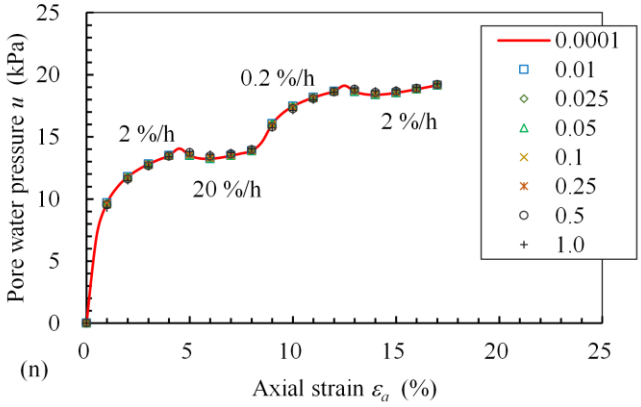

(n)

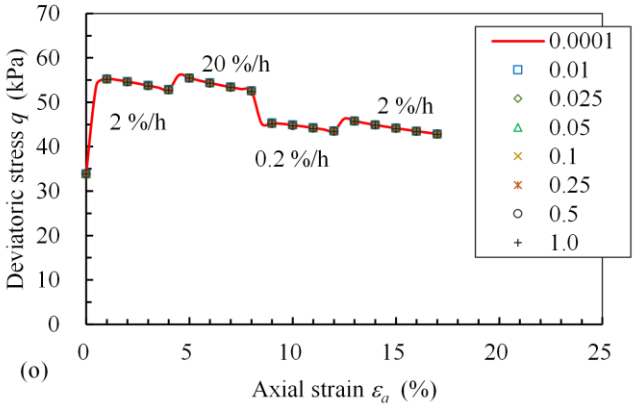

(o)

Figure 6 (*Continued*)

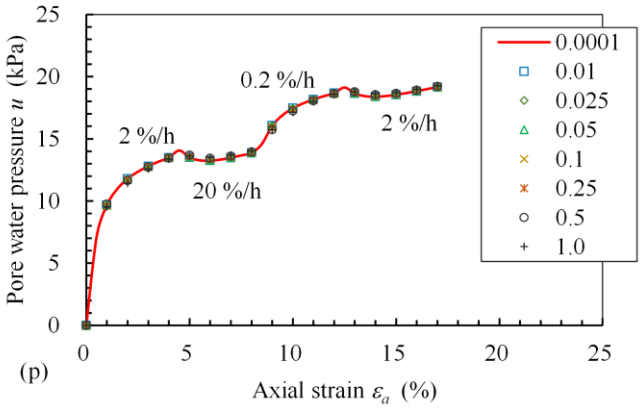

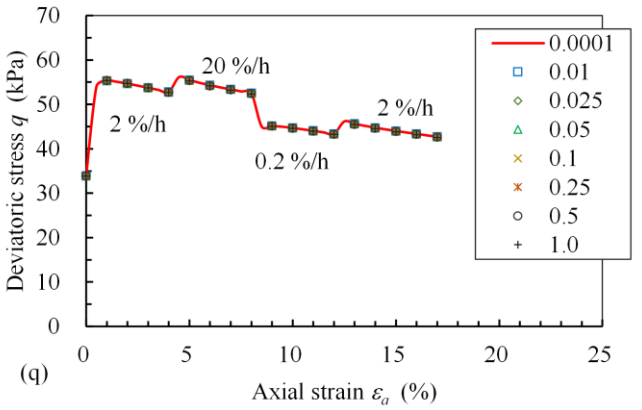

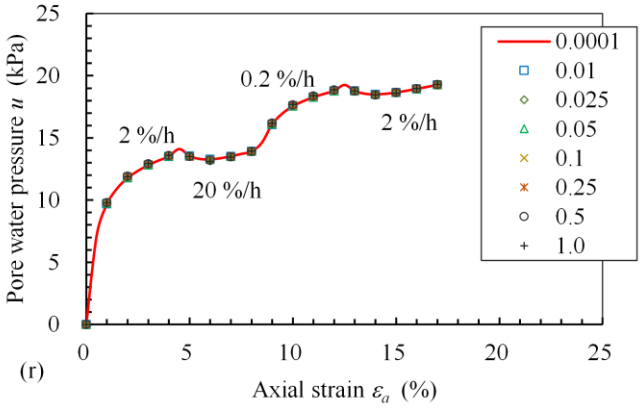

Figure 6 (*Continued*)

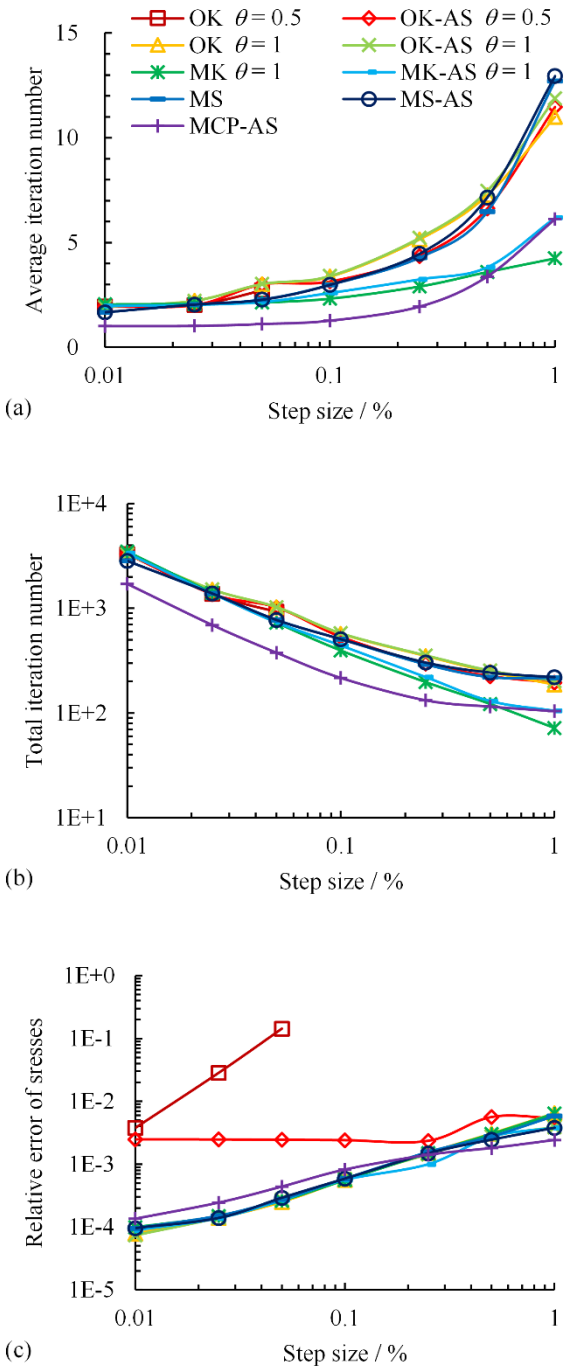

Figure 7 Comparison of simulated results using different incremental steps and time integration algorithms for undrained triaxial step-changed CRS tests for: (a) average iteration number, (b) total iteration number, and (c) relative error of stresses.

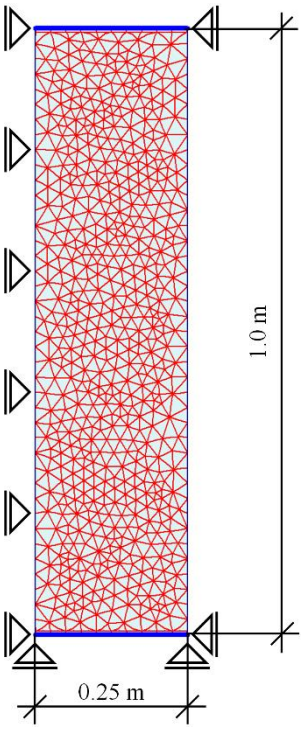

Figure 8 Geometry and boundary conditions used in biaxial test simulation

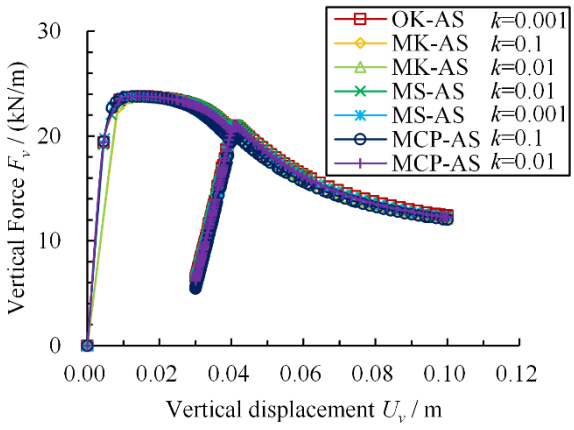

Figure 9 Comparison of simulated results of F_v – U_v for the biaxial test at the top boundary of specimen calculated by different time integration algorithms

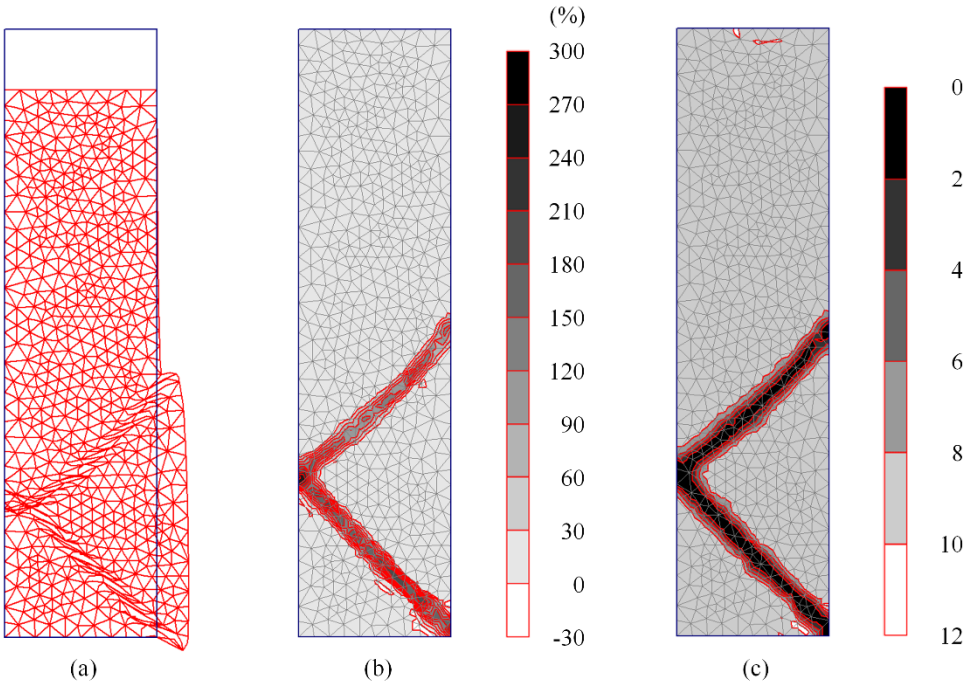

Figure 10 Simulated results by the modified Katona's algorithm (θ = 0.1) with k = 0.01 for biaxial test up to a global vertical strain of 10%: (a) true scale deformed mesh, (b) shading of shear strain, and (c) shading of bonding parameter χ

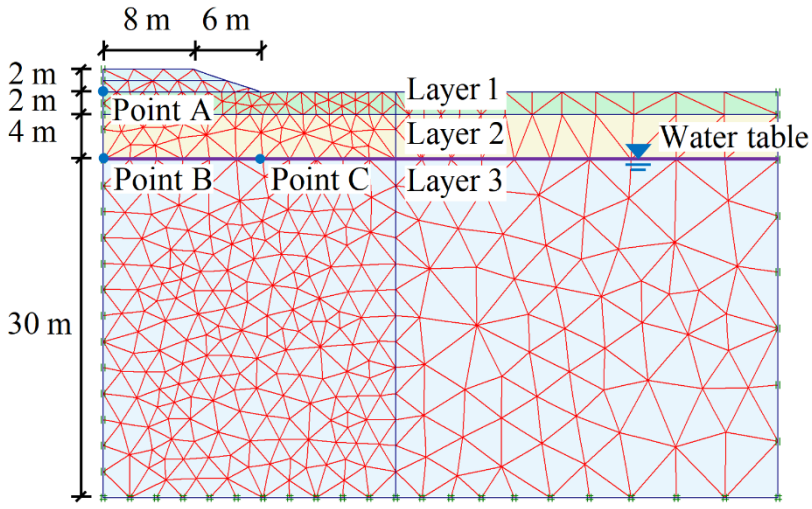

Figure 11 Geometry of benchmark embankment and assumed soil profile

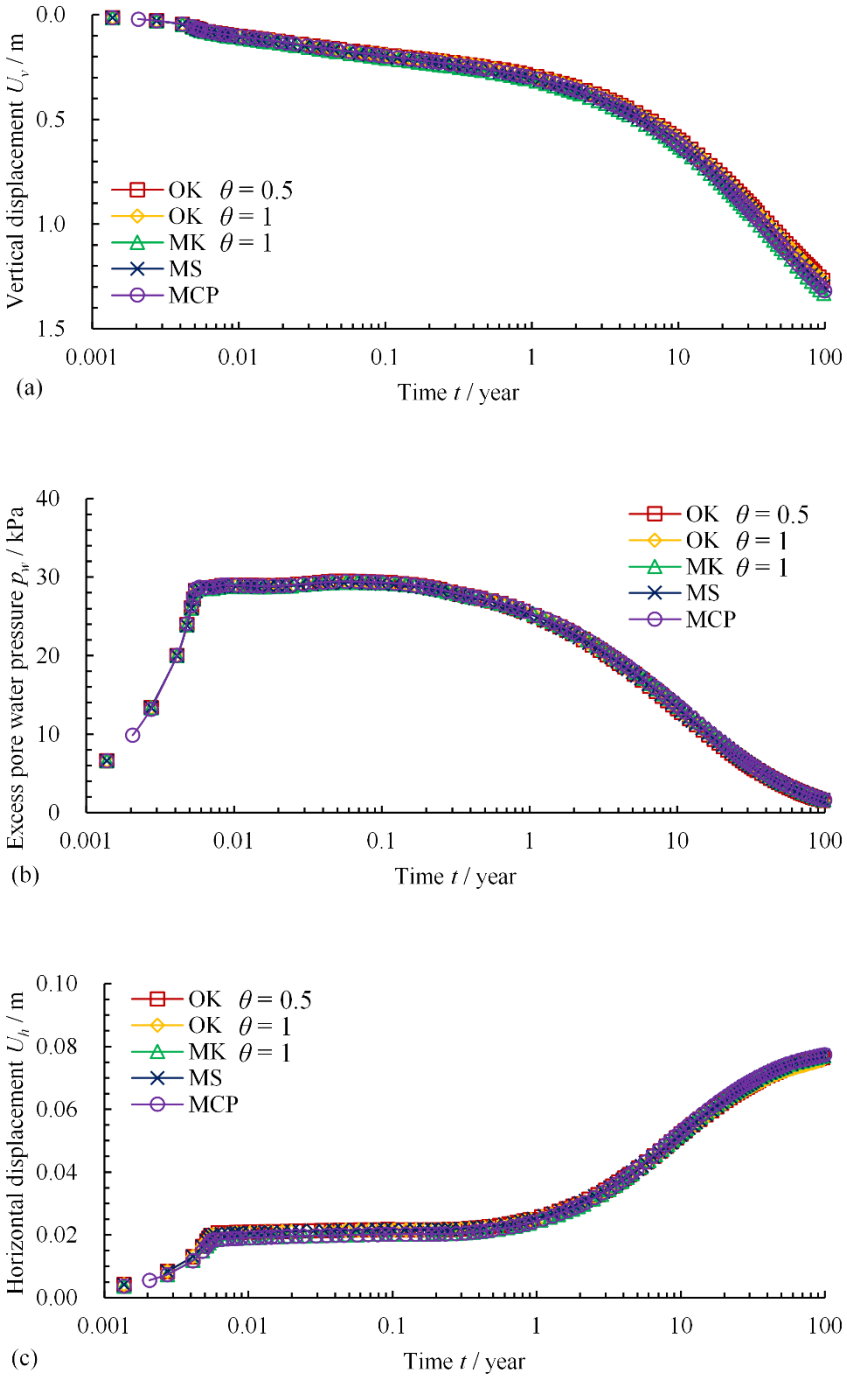

Figure 12 Simulated results of embankment by different time integration algorithms for: (a) vertical displacement U_v at point A, (b) excess pore water pressure p_w at point B, and (c) horizontal displacement U_h at point C

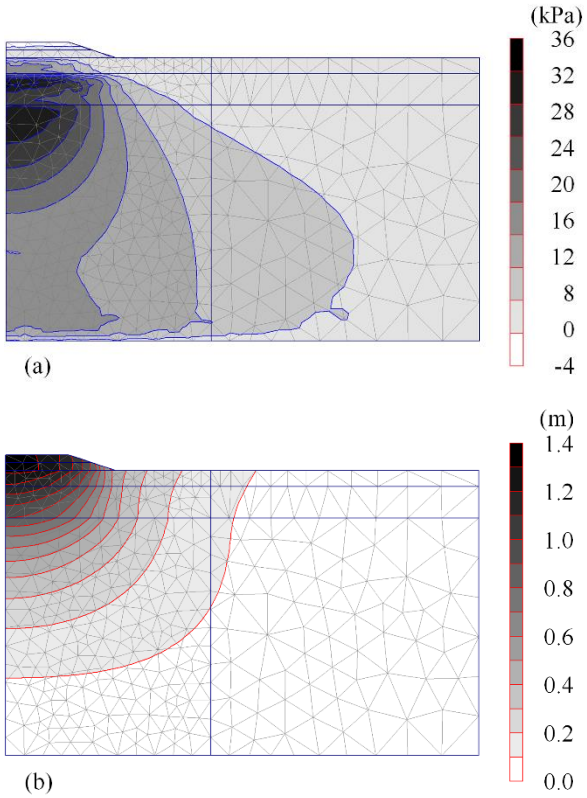

Figure 13 Simulated results of embankment by the modified Katona's algorithm ($\theta = 0.1$) with k = 0.01 for: (a) excess pore water pressure field immediately after construction, and (b) displacement field after 100 years of consolidation

Table 1 Values of model parameters and constants of Wenzhou sensitive clay

Parameter	σ_{p0} /kPa	e_0	υ	κ	λ_i	M	$C_{\alpha ei}$	χ_0	ξ	ξ_d
Value	81	1.89	0.25	0.062	0.294	1.16	0.0078	10	5.5	0.35

Table 2. Global iteration number and CPU time by different time integration algorithms in biaxial test simulations

Algorithm	Comparison items	Substepping parameter k		
		0.1	0.01	0.001
Original Katona (θ = 0.5)	Number of iterations	Failed	Failed	Failed
	CPU time (s)	Failed	Failed	Failed
Original Katona (θ = 1)	Number of iterations	Failed	Failed	2645
	CPU time (s)	Failed	Failed	465.6
Modified Katona (θ = 1)	Number of iterations	2499	2583	/
	CPU time (s)	627.4	717.5	/
Modified Stolle	Number of iterations	Failed	2440	2430
	CPU time (s)	Failed	73.0	85.3
Modified cutting plane	Number of iterations	3032	2634	/
	CPU time (s)	31.9	69.1	/

Note: "/" represents that the simulation has not been carried out.

Table 3. Values of vertical displacement until calculation non-convergence by different time integration algorithms for biaxial test simulations with a target vertical displacement of 0.5 m

Algorithm	Substepping parameter k		
	0.1	0.01	0.001
Original Katona (θ = 0.5)	0.036 m	0.067 m	0.095 m
Original Katona (θ = 1)	0.043 m	0.075 m	0.117 m
Modified Katona (θ = 1)	0.150 m	Finished	Finished
Modified Stolle	0.070 m	0.113 m	0.161 m
Modified cutting plane	Finished	Finished	/

Note: "/" represents that the simulation has not been carried out.

Table 4 Values of model parameters and initial state variables of Poko clay

Layer	POP / kPa	e_0	υ	κ	λ_i	M	$C_{\alpha ei}$	χ_0	ξ	ξ_d	K_0	k / (m/s)
1	30										1.0	1×10^{-7}
2	20	2.1	0.2	0.03	0.26	1.2	0.001	12	9	0.2	0.7	1×10^{-9}
3	10										0.52	1×10^{-9}

Table 5. Global iteration number and CPU time calculated by the model using different time integration algorithms for embankment simulations

Comparison items	Algorithm				
	OK(θ = 0.5)	OK(θ = 1)	MK(θ = 1)	MS	MCP
Number of iterations	856	921	917	882	941
CPU time (s)	150.9	164.7	564.1	131.6	36.3

Table 6. Summary of the performance of different time integration algorithms for comparison

Algorithm	Integration point level	Finite element level	
	Undrained triaxial test	Biaxial test	Embankment
OK (θ = 0.5) without substepping	Poor	Poor	/
OK (θ = 0.5) with substepping	Good	Poor	Fair
OK (θ = 1) without substepping	Good	Poor	/
OK (θ = 1) with substepping	Good	Poor	Fair
MK (θ = 1) without substepping	Good	Fair	/
MK (θ = 1) with substepping	Good	Fair	Fair
MS without substepping	Good	Poor	/
MS Stolle with substepping	Good	Good	Fair
MCP with substepping	Good	Good	Good

Note: Good = both convergence and accuracy are good; Fair = either convergence or accuracy is good; and Poor = both convergence and accuracy are bad; "/" represents that the simulation has not been carried out.

Table A1 State parameters and constants of ANICREEP model for intact natural soft clays

Type	Parameter	Definition	Determination
Modified Cam-Clay parameters	p_{c0}^r	Initial size of reference surface	by $p_c^r = (q_i - p_i'\alpha_{K0})^2 / [(M_c^2 - \alpha_{K0}^2) p_i'] + p_i'$ with p'_i and q_i obtained from $\sigma_h^i = K_0(\sigma_{22}^0 + \text{POP})$ and $\sigma_v^i = \boldsymbol{\sigma}_{22}^0 + \text{POP}$, where POP is the overburden stress (in-situ vertical stress $\boldsymbol{\sigma}_{22}^0$ minus preconsolidation pressure $\boldsymbol{\sigma}_p$ from conventional oedometer test). So POP can be used as input alternatively to replace p_{c0}^r
	e_0	Initial void ratio	From tests of physical properties of the soil
	υ	Poisson's ratio	From initial part of stress-strain curve
	κ	Swelling index	From an oedometer test or a consolidation test
	λ_i	Intrinsic compression index	
	M_c	Slope of CSL in p'-q plane	From conventional drained or undrained triaxial tests in compression
Viscosity parameter	μ	Fluidity of soils	by $\mu = \frac{C_{\alpha ei}(M^2 - \alpha_{K0}^2)}{\tau_r(1+e_0)(M^2 - \eta_{K0}^2)}$ and $\beta = \frac{\lambda_i - \kappa}{C_{\alpha ei}}$ where $C_{\alpha ei}$ is intrinsic creep index from 24h consolidation tests on remoulded sample of the soil and can be used as input
	β	Coefficient of rate-dependency	
Anisotropy parameters	α_0	Initial anisotropy	by $\alpha_0 = \alpha_{K0} = \eta_{K0} - (M_c^2 - \eta_{K0}^2)/3$ with $\eta_{K0} = 3M_c/(6 - M_c)$ (based on Jacky's formula)
	ω	Absolute rate of yield surface rotation	by $\omega_d = \frac{3(4M^2 - 4\eta_{K0}^2 - 3\eta_{K0})}{8(\eta_{K0}^2 + 2\eta_{K0} - M^2)}$ and $\omega = \frac{1+e_0}{\lambda_i - \kappa} \ln \frac{10M^2 - 2\alpha_{K0}\omega_d}{M^2 - 2\alpha_{K0}\omega_d}$
	ω_d	Relative rate of yield surface rotation	
Destructuration parameters	χ_0	Initial bonding ratio	by $\chi_0 = S_t - 1$ where S_t is sensitivity of soil from a shear vane test, or by $\chi_0 = \sigma'_{p0} / \sigma'_{pi0} - 1$ from an oedometer test
	ξ	Absolute rate of bond degradation	From consolidation tests with two different stress ratios $\eta = q/p'$, estimated by $\xi + \xi\xi_d \frac{2(\eta - \alpha)}{M^2 - \eta^2} = \frac{-(1+e_0)}{e^{vp}} \ln \left[\frac{\sigma'_f}{\chi_0 \exp(\frac{e^{vp}}{\lambda_i - \kappa}) \sigma'_{vi0}} - \frac{1}{\chi_0} \right]$
	ξ_d	Relative rate of bond degradation	